Overpressure Protection of Battery Energy Storage Systems (BESS)

1D Explosion Dynamics to Model BESS Deflagration

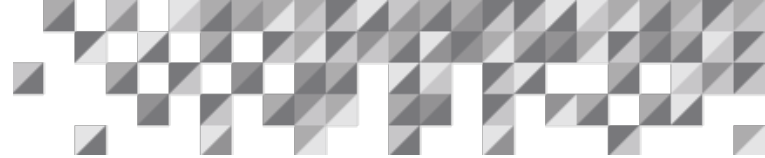An ioMosaic White Paper

Date: September 6, 2023

James Close

close.j.uk@ioMosaic.com

Charles Lea, P.E.

lea.c.mn@ioMosaic.com

1. Introduction

Increased awareness of sustainable development objectives is encouraging the uptake of different energy storage media. Technologies are also now rapidly developing to a point where they can be a practicable alternative to combustion engines for public and private modes of transport. Lithium-ion (Li-ion) batteries are one technology widely used to meet those targets, for use in electric vehicles and energy storage installations. There is competition to improve battery and system performance by increasing energy capacity, improving the battery lifespan, and investing in battery management systems. This competition is driving the increase in Li-ion batteries (LIBs) production volumes, with current estimates in the range of a few million tonnes per year to the equivalent of 130-225 GWh/y with the aim to de-carbonise society and meet the sustainability targets described in the UN Sustainable Development Goals 7,8,12 and 13 (1,2).

As outlined in the US Department of Energy's national energy blueprint, Li-ion batteries accounted for 98% of the commissioned stationary storage facilities (battery energy storage systems) (3). This plan focuses on higher cell production in the US, enhancing and supporting supply chains, and funding additional research into new battery technology.

As shown in Figure 1, there are various types of energy storage systems based on application. The use of Battery Energy Storage Systems (BESS) is gaining traction in the US market because they have high energy densities and can store large quantities of energy within a small footprint 90-190 Wh/kg depending on the cell type (4,5).

## Figure 1: Positioning of energy storage technologies
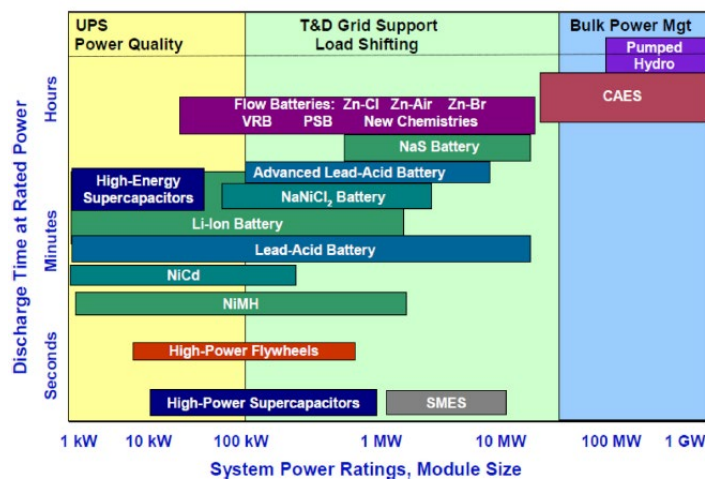
Source: AL Shaqsi AZ, Sopian K, Al-Hinai A. Review of energy storage services, applications, limitations, and benefits. Energy Reports [Internet]. 2020;6:288–306. Available from: https://doi.org/10.1016/j.egyr.2020.07.028
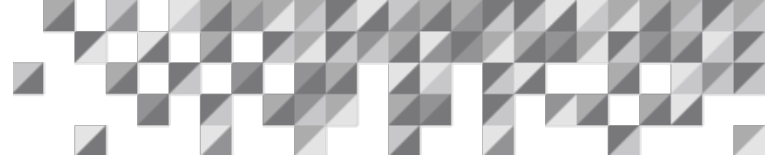
BESS are also gaining wide use to support decarbonization, integrating a diverse group of energy resources to meet energy demand created by urban populations and economic growth (5). To meet both objectives, the energy supply needs to be balanced and reliable. With the variety of energy sources such as wind and solar, changes in weather conditions, energy supplies to local populations may not be reliable. BESS systems provide a mechanism in which energy can be stored and supplied during peak periods if the greener energy systems are unable to meet peak energy demands at different times (5–7).

BESS systems are now increasingly utilized by regional grid operators, as shown in Figure 2 (8). With greater production and application of Li-ion BESS, the inherent hazards are more apparent with more frequent use. This white paper will explore the mechanics of deflagrations that can occur during a thermal runaway event in a BESS and how Process Safety Office® SuperChems™ can be used to size deflagration vents to protect against such explosions in elongated geometries.

Figure 2: Large-scale battery storage capacity by region (2010-2019)
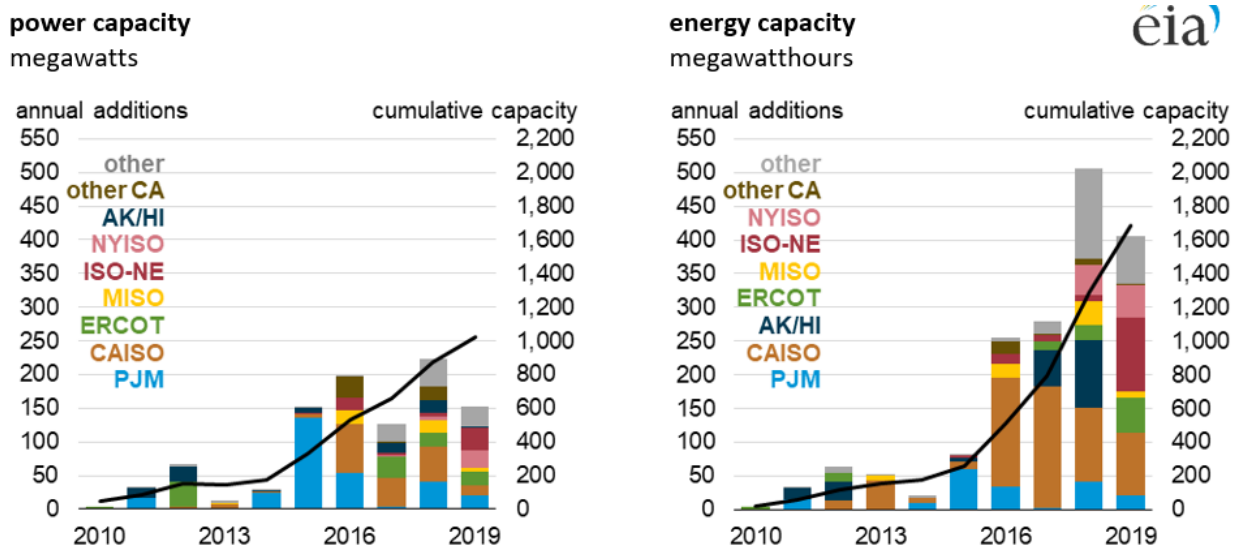
Source: U.S. Energy Information Administration, 2019 From AIE-860, *Annual Electric Generator Report*
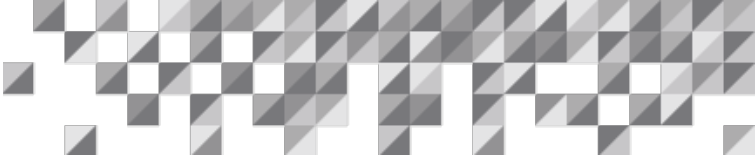
2. BESS Building Blocks

2.1 What is a Li-ion Battery and how are they integrated into a BESS?

Lithium-ion batteries (LIBs) store and discharge energy via the principles of electrochemistry. A LIB cell contains electrodes, an electrolyte and a separator, which prevents the connection of the electrodes creating an internal short circuit. The positive electrode (cathode) is made from lithium metal oxide, and the negative electrode (anode) is made from graphite intercalation compound (LixC6). The redox reactions are described in Figure 3 below, where the state of charge (SOC) and discharge is directed via the movement of Lithium ions through the electrolyte and separator to be intercalated into the negative and positive electrode generating currents.

Figure 3: Energy storage mechanism of a Li-ion Battery
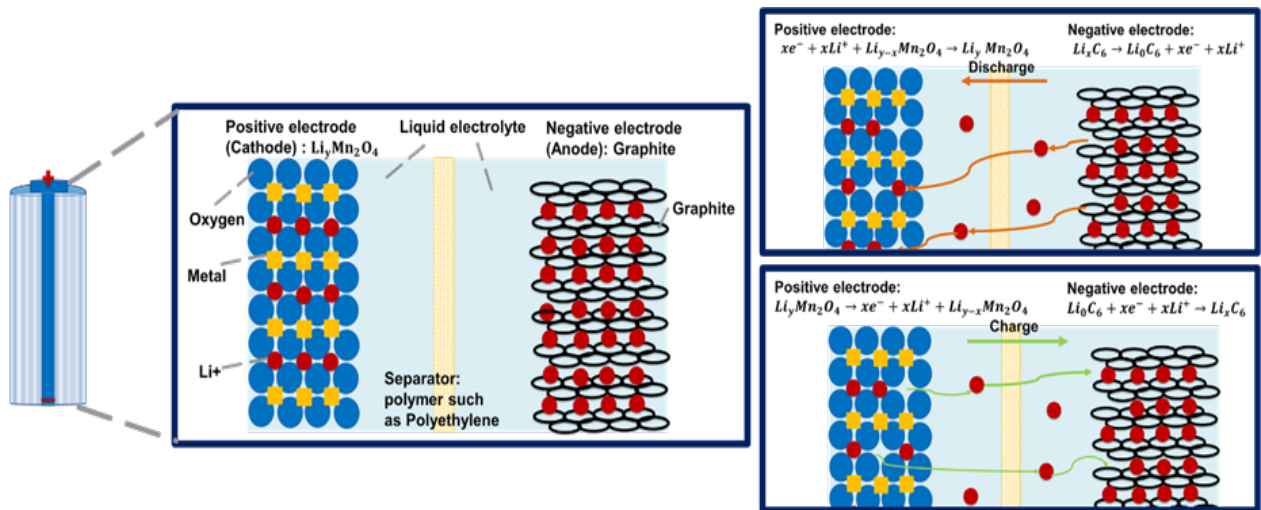
Source: ioMosaic Corporation

Cells come in these main formats; cylindrical (18650 type 65mm in length and 18mm in diameter), prismatic, and fin/pouch, as shown in Figure 4 a) each with its chemistries, benefits, and disadvantages, such as capacity, size and ease of modularization. These cells are then arranged in a module configuration which makes up a larger battery pack and management system, as illustrated in Figure 4 b) (9).
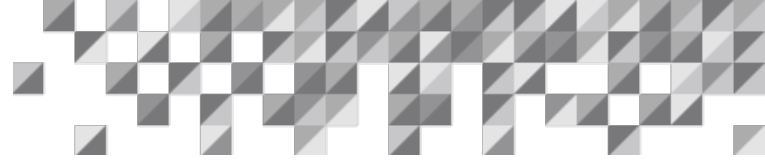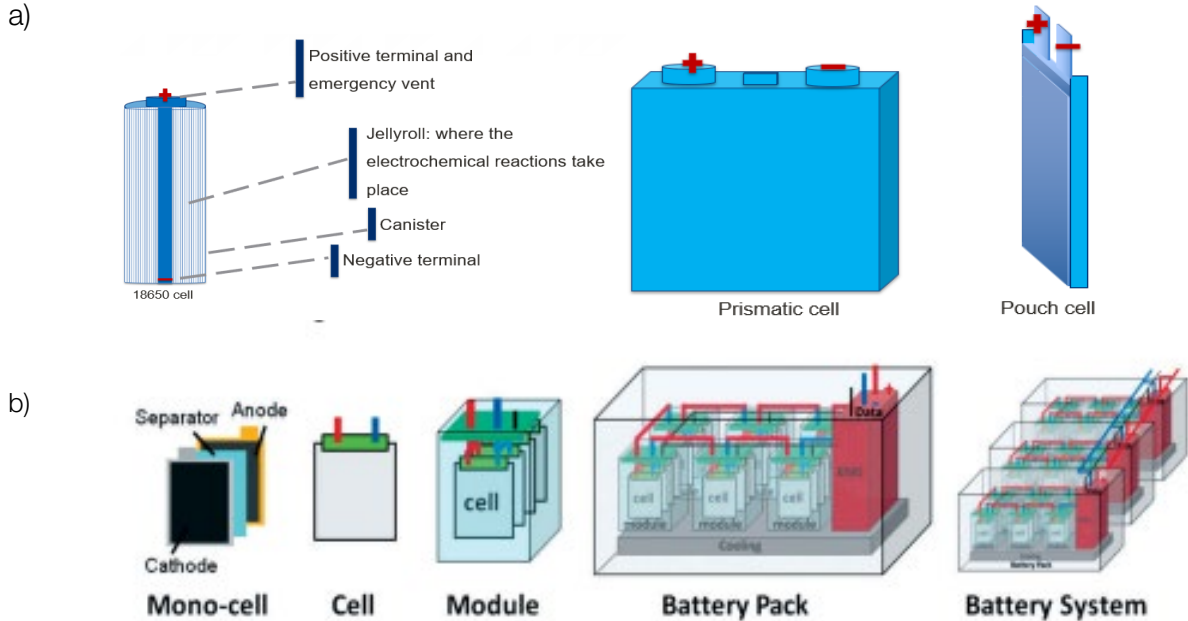
Figure 4: Sketches of different cell types and Modularization

a)

b)

Source: a) ioMosaic Corporation and b) A. Otto, S. Rzepka, T. Mager, B. Michel, Fraunhofer, C. Lanciotti, T. Günther OK. Advanced Microsystems for automotive applications 2012. Battery Management Network for Fully Electrical Vehicles Featuring Smart Systems at Cell and Pack Level. 1st ed. G Meyer, editor. Springer; 2012. 18–24 p.

Battery energy storage systems have many designs, configurations, control, and safety control systems depending on the end-user and the manufacturer. Currently a Tesla powerpack consists of modules containing 900 18650 cells, with 16 modules in a power pack. The multiple power packs can be installed side-by-side and housed in an enclosure, as shown in Figure 4 (10).

The battery packs are aligned with an installed battery management system that monitors conditions such as battery lifespan, temperature, current and voltage. Depending on the battery pack design used, there are cooling methods such as using coolant pumps, pumping ethylene glycol between modules, reservoirs, fans and radiators for temperature control (10). Outside the battery pack unit, this power conversion, auxiliary and control subsystems (11). The power conversion subsystem controls energy transfer to and from the electrical supply using an inverter /charger. The Auxiliary system includes equipment to perform auxiliary functions such as temperature control, ventilation, and fire suppression (11). Finally, the control subsystem monitors the battery management system and will include communication and protection subsystems (11). A more detailed layout of a battery energy storage system can be seen in Figure 5.
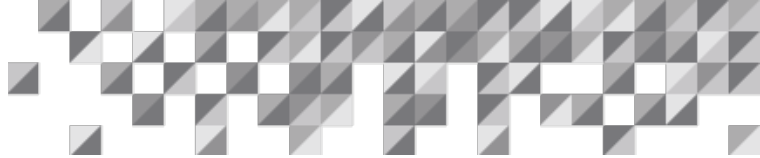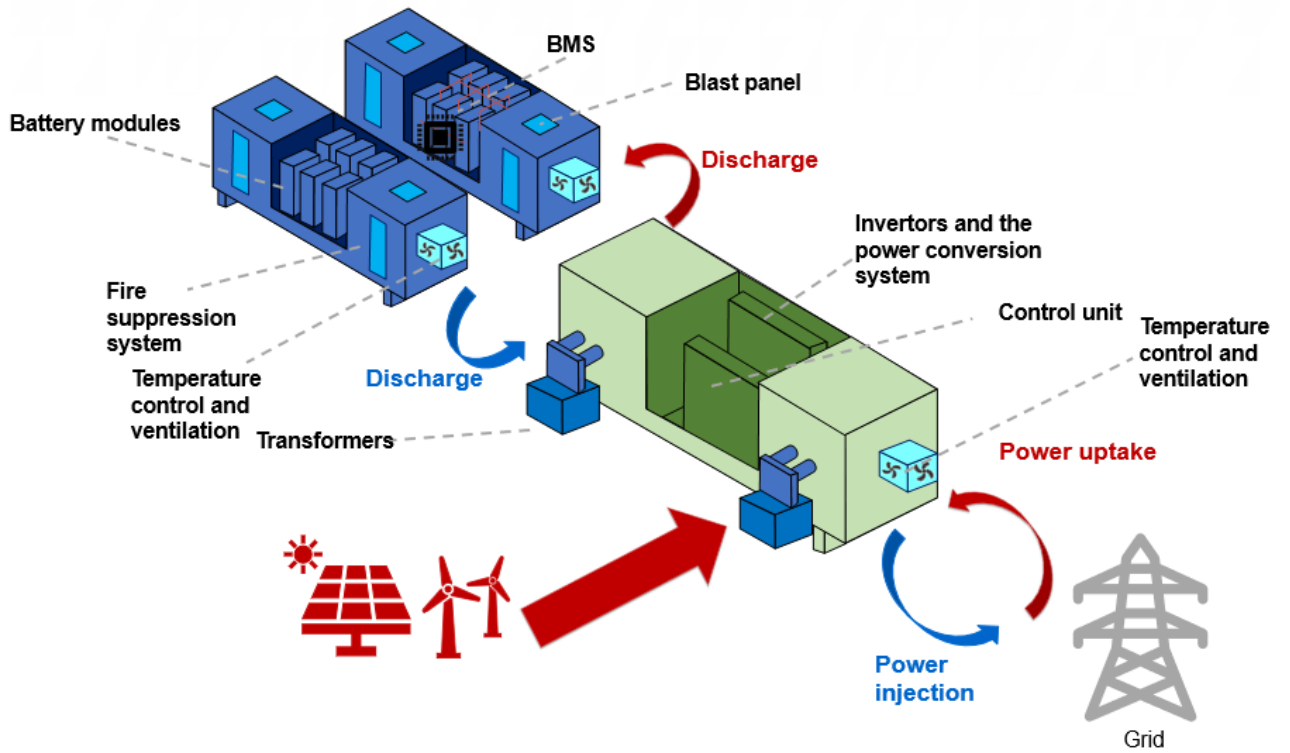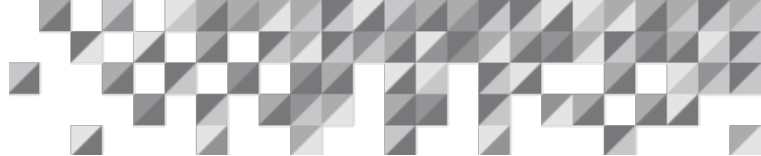
Figure 5: General layout of a BESS

Source: ioMosaic Corporation

3. Inherent Hazards of BESS Systems

LIBs are thermally unstable and can result in fires or explosions. These hazards result from releasing toxic and flammable gases and particulates. Progression of a runaway reaction is difficult to predict given the many possible interactions, typically requiring multiple tests and models for design and implementation. However, safety issues for LIBs can be generalized to the following (12):

1. Thermally unstable cathode
2. Flammable electrolyte
3. Fragile separator
4. Overcharge-sensitive cathode/anode
5. High sensitivity to metallic elements

LIBs are sensitive to high temperatures and contain highly flammable materials. Li-ion batteries tend to degrade, and when the material such as the cathode, electrolyte and even current collectors are exposed to oxygen at a higher temperature, they ignite and burst into flames due to autocatalytic reactions. These events are driven by a thermal runaway process, which will be explored in the following sections. Hazards during the thermal runaway process include but are not limited to (12–15):

1. Electrolyte reactions
2. Separator melting
3. Short circuits/generation of sparks
4. Extreme heat generation
5. Toxic gas and particulate release
6. Fires
7. Explosions

3.1 Li-ion Battery Thermal Runaway

Due to their high energy density, LIB cells contain a significant amount of energy. However, the solid-electrode interface (SEI) at the electrodes tends to begin to decompose at a temperature of between 90-120℃. Higher temperatures make the cell more unstable and result in the anode and cathode decomposing via oxidation in the presence of the electrolyte at around 130-200℃, depending on the internal chemistry (17,18–20). Finally the electrolyte begins to decompose at around 200-300℃ (12). At this temperature range, the decomposition of the multiple components begins to progress, providing a pathway for thermal runaway, the steps of which are outlined graphically in Figure 6. The process of thermal runaway can occur via other abuses, thermal, mechanical, electrical and ageing/defects of the cell (11,13,16).
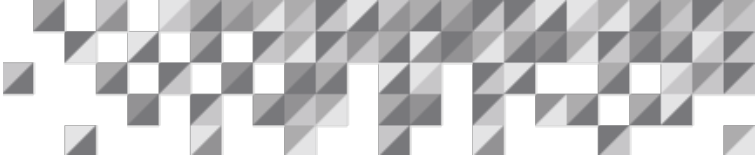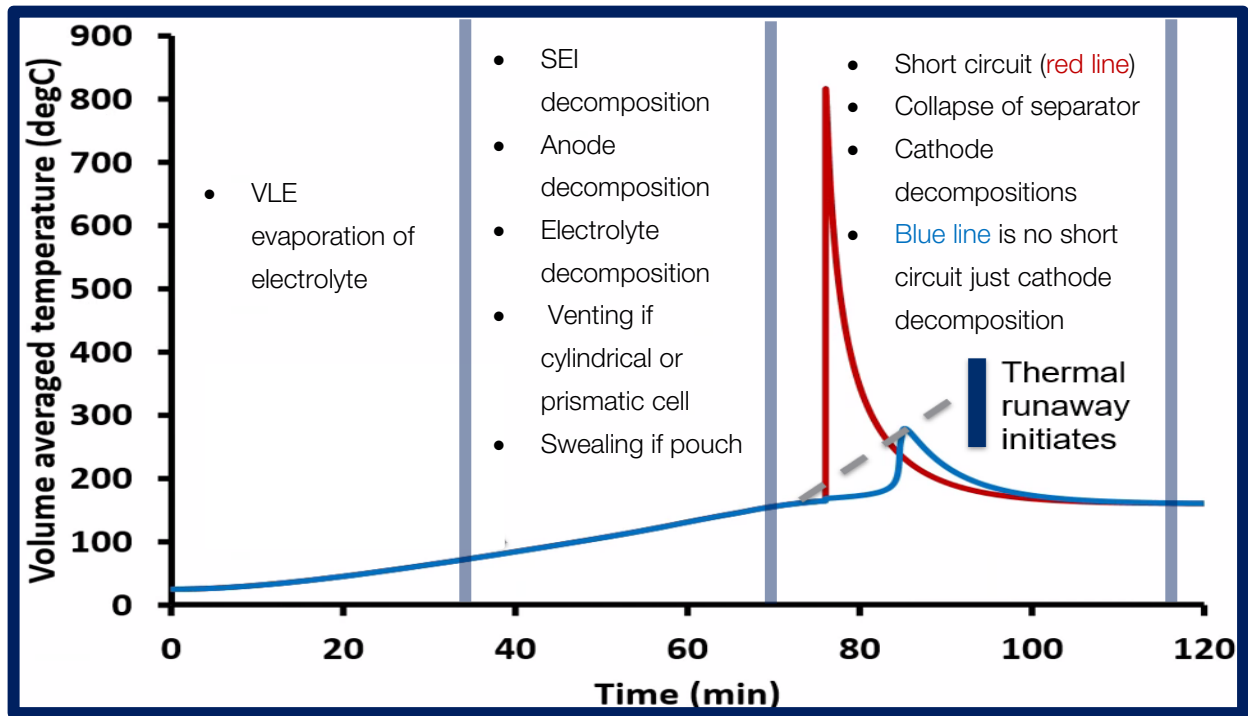
Figure 6: Steps of Li-ion cell thermal runaway

Source: ioMosaic Corporation

Thermal and electrical abuses such as hot weather conditions, fires, overcharging of a cell, and external and internal short circuits can generate enough heat, starting decomposition reactions of the SEI layer, the anode and then finally the cathode. Mechanical failure can result in the separator breaking causing a short circuit, and depending on capacity and the state of charge, the cell can release a large amount of energy (13,16,18,19). Certain mechanical failures involve nail penetration or simple crushing of the cell can.

Over a battery's life cycle the performance will decrease and will become less safe. Wear and tear may compromise safe operation, but also can be attributed to the formation of Lithium-ion dendrites and electrode surface changes. Lithium dendrites form at the negative electrode during the charging process (20). During Li-ion movement, the ions can accumulate on the anode surface (20). This accumulation can be characterized as metallic spines that can pierce the separator, resulting in an internal short circuit and causing thermal decomposing of its components, as shown in Figure 7. The age of the cell plays a vital role as this can affect capacity from a performance perspective but can potentially make cells unsafe, especially when Lithium dendrites form at the electrode.
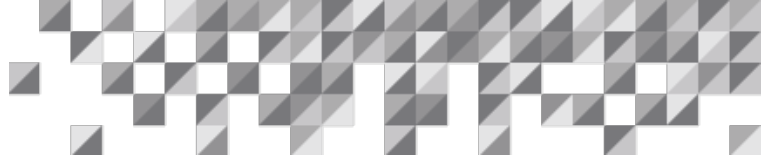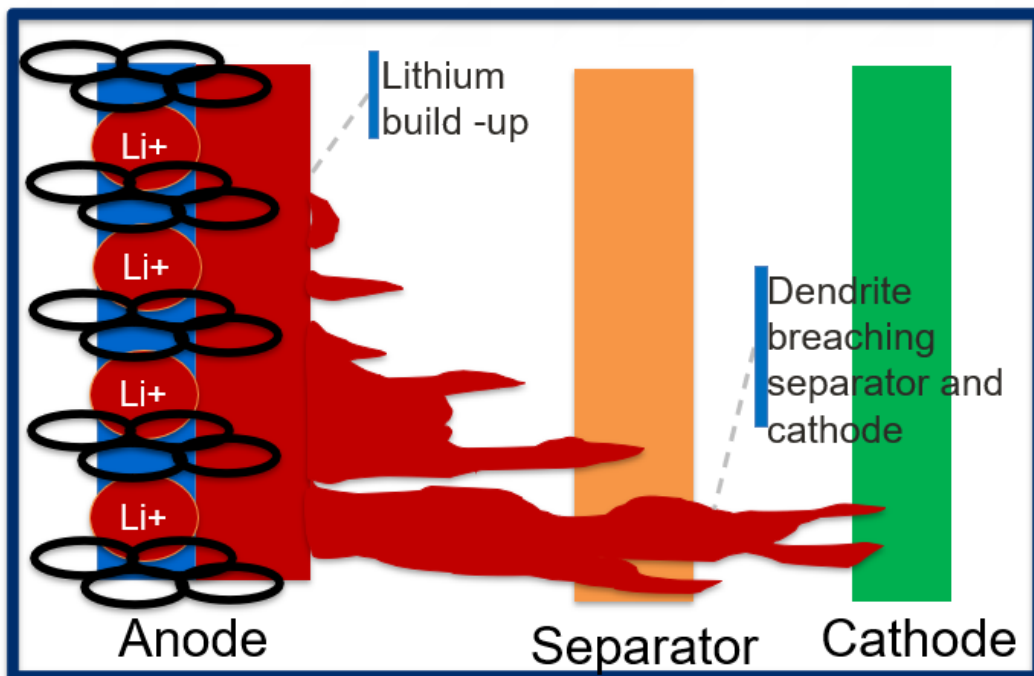
Figure 7: Steps of Li-ion cell thermal runaway

Source: ioMosaic Corporation

Due to the unstable nature, high energy densities of the Li-ion cell and small production differences between cells, the different chemistries will have different inherent hazards. Positive electrode chemistry is very important to understand, as some compounds are more unstable than others. As shown in Figure 8 LFP cells (electrode: $LiFePO_4$) have a lower energy density and therefore, a higher onset and lower peak temperatures compared with LCO and NMC electrodes (21). Although LFP are safer, this is at the cost of capacity and footprint, which may be appropriate for energy storage systems but not used frequently in electric vehicles.
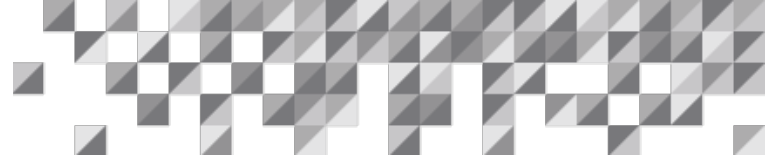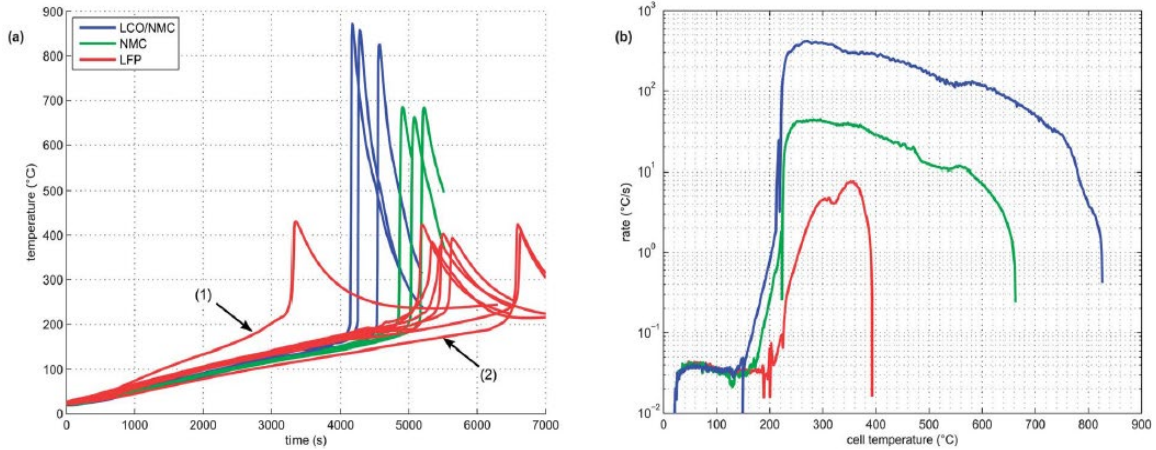
Figure 8: Runaway experiments of different Li-ion battery chemistries

A single cell is hazardous; in a module or a rack of cells, the thermal runaways can propagate between cells resulting in venting hazardous substances, fire, and when confined, explosions of a larger magnitude, as shown in Figure 9.

Source: Golubkov AW, Fuchs D, Wagner J, Wiltsche H, Stangl C, Fauler G, et al. Thermal-runaway experiments on consumer Li-ion batteries with metal-oxide and olivin-type cathodes. RSC Adv. 2014;4(7):3633–42.

Figure 9: Thermal runaway propagation between cells including venting through the burst disc

a) Single cell

b) Thermal runaway propagating in module

c) Thermal runaway propagating between modules
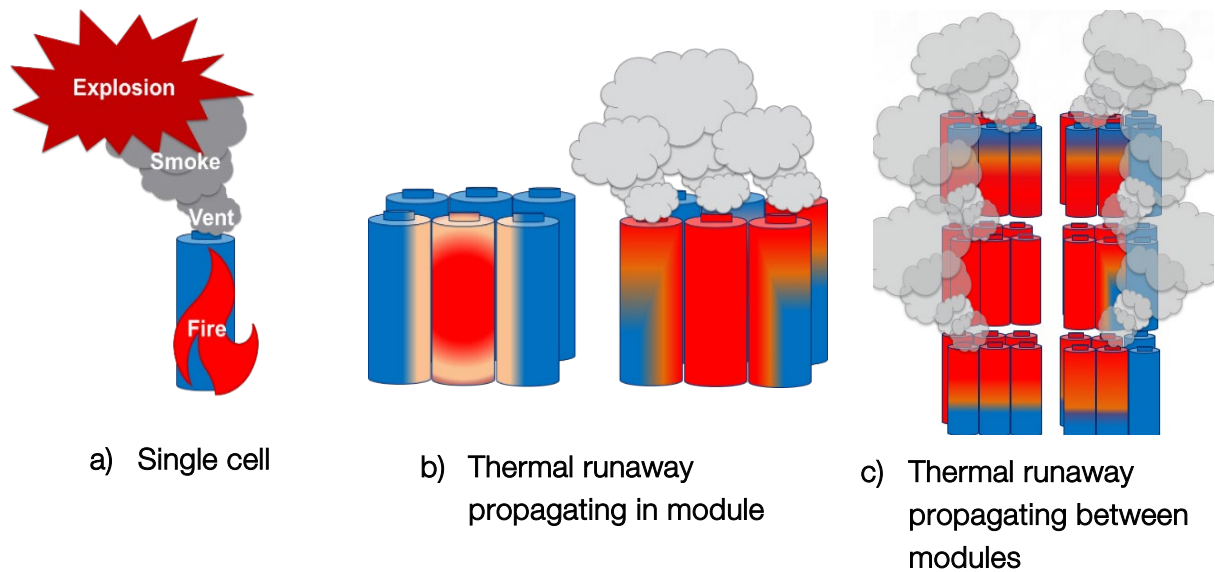
Source: ioMosaic Corporation
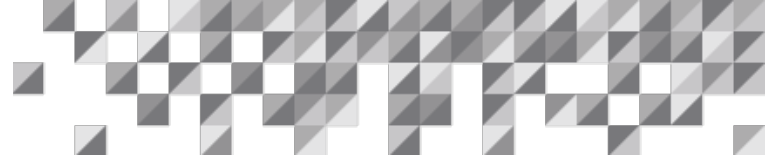
3.2 Li-ion Battery Vent Gases

When a LIB reaches a specific temperature, vaporization of the electrolyte begins to occur. Some lithium-ion batteries, such as cylindrical cells of type 18650 or 21700, have a vent cap (similar to a ruptured disc on a reactor) which, once a maximum pressure is reached will bur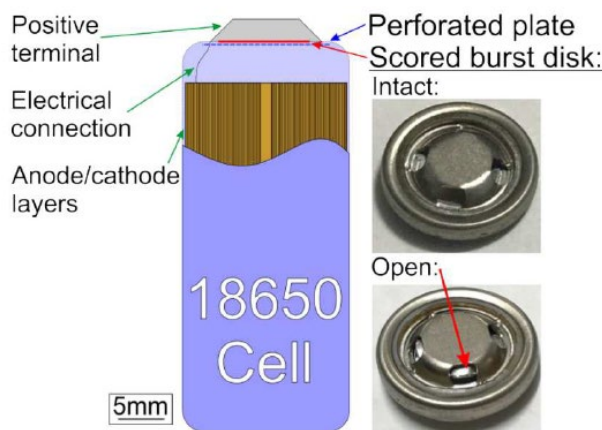st, ejecting vent gases, vaporized electrolyte and solid ejecta (16,22–26). The vent cap of a 18650 cell is shown below in Figure 10 (23).

Figure 10: Burst disc of an 18650 cell

Source: Austin Mier F, Hargather MJ, Ferreira SR. Experimental Quantification of Vent Mechanism Flow Parameters in 18650 Format Lithium Ion Batteries. J Fluids Eng Trans ASME. 2019;141(6).
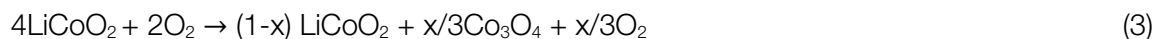
The extreme heat generated in the housing where the cells are cased is released, and the venting material can escape via that route. Standard electrolytes are LiPF6 salt and ethylene carbonate (EC) solution. Other organic co-solvents are components such as Propylene Carbonate (PC), Dimethyl Carbonate (DMC), Ethyl Methyl Carbonate (EMC) and Diethyl Carbonate (DEC) (27).

When oxygen is released from the decomposition reaction of the electrodes, electrolyte combustion reactions occur, resulting in flammable and toxic gases such as Oxygen (O_2), Hydrogen (H_2), Carbon Monoxide (CO), Carbon dioxide (CO_2), Methane (CH_4), Ethyne (C_2H_2), Ethylene (C_2H_4), Ethane (C_2H_6), and other hydrocarbons (18,21,25,27–32). In other experiments, electrolyte vapours, Hydrogen Chloride and Hydrogen Fluoride were also detected in the apparatus (27).

It has been shown in gas chromatography experiments that the lower the state of charge, the lower the proportion of gases such as ethylene or C4-C5 hydrocarbons (31). The level of more significant hydrocarbons has also been proven to vary depending on different chemistries, formats, and states of charge. Please see Appendix A for an overview of different components that can be released.
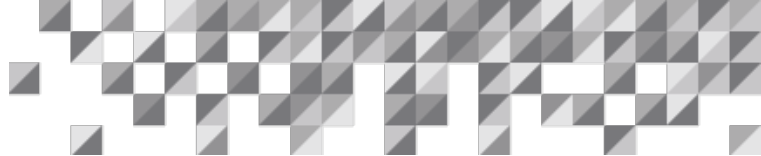
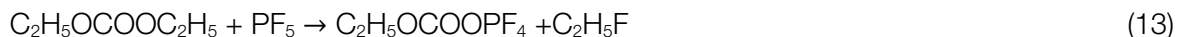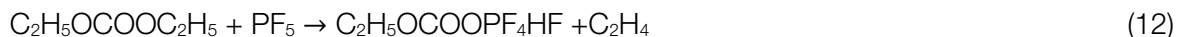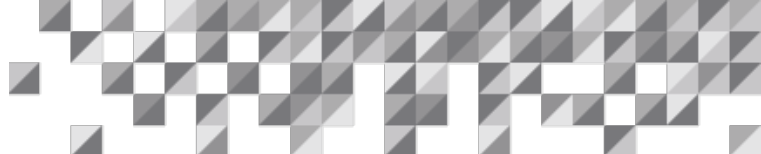Some reactions that occur during the combustion and venting process can be seen below. Equation 1 to 2 describes the SEI decomposition with the electrolytes (33,34). When the SEI decomposition occurs, this elevates the temperature past the electrode decomposition onset temperature and creates a chain of reactions. When the metal oxide electrodes such as LCO decomposes to intermediate compounds releasing Oxygen and potentially providing more mechanisms for further reactions with the electrolyte; this is shown in equations 3 – 9 (34–40).

$$2Li + C_3H_4O_3 \text{ (EC)} \rightarrow Li_2CO_3 + C_2H_4 \tag{1}$$

$$2Li + C_4H_6O_3 \text{ (PC)} \rightarrow Li_2CO_3 + C_3H_6 \tag{2}$$

$$4LiCoO_2 + 2O_2 \rightarrow (1\text{-}x) \, LiCoO_2 + x/3Co_3O_4 + x/3O_2 \tag{3}$$

$$Co_3O_4 \rightarrow 3CoO + 1/2O_2 \tag{4}$$

$$Co_3O_4 + 1/2C \rightarrow 3CoO + 1/2CO_2 \tag{5}$$

$$CoO \rightarrow Co + 1/2O_2 \tag{6}$$

$$2LiCoO_2 + CO_2 \rightarrow Li_2CO_3 + 2Co + 3/2O_2 \tag{7}$$

$$5/2O_2 + C_3H_4O_3 \text{ (EC)} \rightarrow 3CO_2 + 2H_2O + \text{Heat} \tag{8}$$

$$4O_2 + C_4H_6O_3 \text{ (PC)} \rightarrow 4CO_2 + 3H_2O + \text{Heat} \tag{9}$$
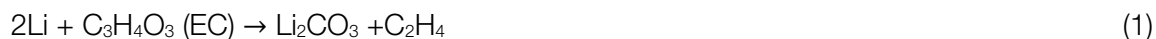
Hydrogen fluoride gas being emitted depends on the electrode binder and electrolyte slat being used, for electrolytes such as DEC containing Lithium Hexafluorophosphate salt can breakdown as shown in equations 10-17 (13,33,34,41).

$$LiPF_6 \leftrightarrow LiF + PF_5 \tag{10}$$

$$LiPF_6 + H_2O \leftrightarrow LiF + HF + POF_3 \tag{11}$$

$$C_2H_5OCOOC_2H_5 + PF_5 \rightarrow C_2H_5OCOOPF_4HF + C_2H_4 \tag{12}$$

$$C_2H_5OCOOC_2H_5 + PF_5 \rightarrow C_2H_5OCOOPF_4 + C_2H_5F \tag{13}$$

$$C_2H_5OCOOPF_4 \rightarrow CO_2 + C_2H_4 + POF_5 + HF \tag{14}$$

$$C_2H_5OCOOPF_4 \rightarrow C_2H_5F + CO_2 + POF_5 \tag{15}$$

$$C_2H_5OCOOPF_4 + HF \rightarrow PF_4OH + CO_2 + C_2H_5F \tag{16}$$

$$C_2H_5OH + C_2H_4 \rightarrow C_2H_5OC_2H_5 \tag{17}$$

We note that cell venting is a dynamic process, the majority of current literature provides snapshots or gas collection experiments but does not provide a clear description of the dynamics generation of the combustion process and vent gas generation. This is a knowledge gap which should be investigated with further research.

3.3 Fire Hazards

During thermal runaway, the release of flammable gases and the decomposition reactions occurring release high amounts of energy and can be up to 79% of the cell's total energy (42). The release of this much energy and the cell reaching temperatures of 400 to 900 ℃, depending on the battery type and state of charge, could result in the individual cells, modules and then packs beginning to catch fire. The vent gases discussed in section 3.2 collectively have a lower flammability limit (LFL) and an upper flammability limit (UFL), which is the concentration of the vent gases in an ignited air mixture.

Experiments have shown that the flammability and high temperatures combustion depend on the kind of electrolytes used. Table 1 shows the flammability limits for batteries with different cathode chemistries (29). LFP cell changes greatly depending on the state of charge, again proving the necessity of battery testing as two battery chemistries and thermal runaway events are not the same.

Table 1: LFL and UFL for ignition of different cell types

Battery type	LFL at SOC<100%	LFL at SOC=100%	LFL at SOC >100%
LCO	4.4	6.2	5.4
LFP	11.7–36.6	7.7	8.2–8.7
NMC	3.9	6.4–7.7	---
Battery type	UFL at SOC<100%	UFL at SOC=100%	UFL at SOC >100%
LCO	85.1	87.1	87.3
LFP	90.6-91.1	89.8	90.4-91.1
NMC	84.9	88.5-90	---

3.4 Explosion Hazards

When LIBs go into thermal runaway, gases are released and are either burned, creating a flame jet or fire. Alternatively, the gases and solid ejecta can accumulate, resulting in gas or combustible dust explosion.
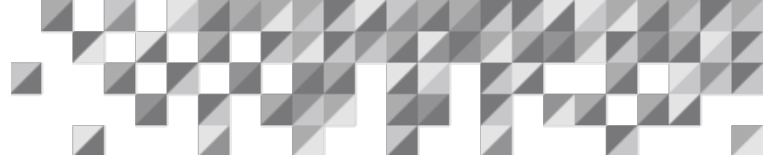
There are two types of explosions for LIBs: internal and external. Internal is where an explosion occurs within the cell casing. The resulting pressure rises can result in the cell rupturing and bursting. This could be due to a safety vent malfunction on cylindrical and prismatic cells (43).

A gas and combustible dust explosion are where there is delayed ignition of the accumulated gases and solid ejecta. An external explosion can be more severe than cell case explosions (43). External explosions will result in multiple cells going into runaways, such as in a battery pack or rack. The gases and solid particulates can then disperse and accumulate in higher concentrations, and due to more cells going into a thermal runaway in the pack, it is not long before highly concentrated gases find an ignition source.

Some experimental work has been conducted to determine some of the explosion severity and the vent gases' upper and lower limits (LEL and UEL) from cell runaway.

Experiments show that for the 18650 cell that the methane and hydrogen volume fractions exceed the lower explosion limits for their respective species. However, depending on the state of charge, it was found that the ratio of flammable gases, in particular, Hydrogen to CO_2 will directly affect the explosion limit (44). The higher the SOC, the thermal runaway becomes more intensive and as shown in previous sections, there is a more significant release of unsaturated hydrocarbons; therefore, cells at higher SOC will always be at greater risk of lower safety and a greater risk of external combustion of vented materials (31).

Combustible solids/ejected contents of Li-ion batteries also are a hazard. Solid material from the electrode winding can be discharged from the melted casing, and the vent cap (42) is also discharged along with vaporized electrolyte and vented gases as the electrodes begin to break down. The combustible dust could be swept away with the vent gases and ignite, creating a dust cloud explosion. Experiments have shown that approximately 68 wt% of the powder ejected from the battery during thermal runaway is carbon. The remaining composition is carbonates, metals and metal oxide (34). Ejected metals and metal oxides pose a safety risk as they require lower energy amounts to ignite and have severe consequences during thermal runaway propagation between cells.

3.5 BESS Code and Standards Overview

When manufacturing and installing a battery pack, regulations such as UL 1741, UL 1973 and IEC 62109 must be adhered to. Additionally, the pack must be designed to comply with UL 9540 and IEC 62619 (10). UL1741 outlines a new safety test standard that certifies products that need to meet the requirements of safe operation in support of grid modernization efforts (45). UL1973 covers battery use in light electric rail and stationary applications such as energy storage applications.
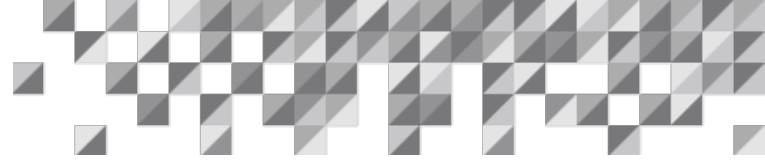
UL1973 provides safety design parameters and the requirements for safety performance tests such as overcharge tests, short circuit tests, temperature and operating limit tests (10,18,46). For batteries used for energy storage systems, UL1973 also requires two fire tests: the first is an external fire test, and the second is an internal fire test (46). IEC 62619 specifies requirements and tests for the safe operation of secondary lithium cells and batteries used in industrial applications including stationary applications (47).

UL9540 has had a major revision which is listed under UL9540A and is the most applicable standard for energy storage systems. It covers the following (48,49).

- Safety of the battery system
- Functional safety
- Fire detection & suppression
- Containment
- Etc..

UL9540A separates the testing requirements into 4 stages (which is outlined in Figure 11). The revised standard (UL9540A) emphasizes the importance of understanding the composition of gases ejected from cells during runaway, ignition, and deflagration hazards (49). The placement and sizing of blast vents is explored in this paper in later sections.

Figure 11: Testing hierarchy in UL 9540A
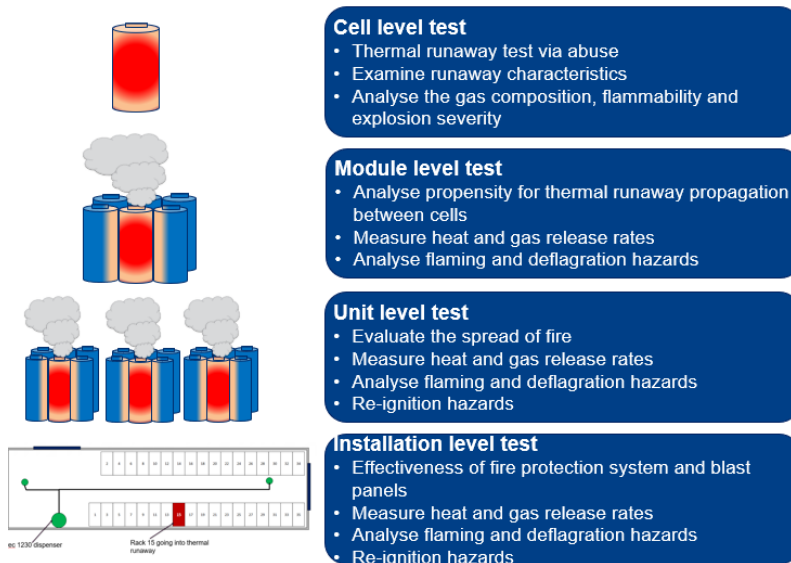
Source: Graphic from ioMosaic Corporation and information from UL9540A energy storage testing method
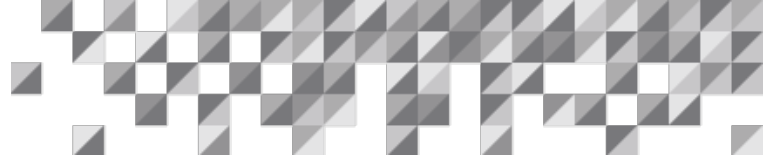
4. Li-ion Cell Thermal Runaway Incidents

Many thermal runaway experiments and models have been used to characterize thermal hazards in LIBs. However, real-life examples will always provide case studies and safety lessons to improve cell design and mitigation strategies. Table 2 below provides a list of some runaway incidents caused in the transportation and mobile phone sector (50).

Table 2: Thermal Runaway Incidents

Classification	Date	Location	Description
Mobile telephones	2016.8.24	Korea	The first explosion of a Samsung Note 7 in the world
	2016.10.14	China	A Huawei P9 exploded during charging
	2016.10.17	Australia	An iPhone 7 caught fire which then, burned a car
	2018.1.9	Switzerland	An iPhone exploded when replacing the battery, which caused an injury and seven poisonings
	2018.12.30	America	An iPhone XS Max self-ignited and burned the user
Electric vehicle	2017.1.15	China	An EV bus self-ignited during driving
	2017.2.19	China	A Tesla Model X caught fire after crashing
	2018.3.24	America	A Tesla Model S caught fire whilst stationary
	2018.5.21	China	An EV bus self-ignited during driving
Airplane	2010.9.3	The UAE	A Boeing 787 crashed due to the battery catching fire, which caused two deaths
	2013.1.7	America	The battery pack caught fire and filled the cabin of a Boeing 787 with smoke
	2013.1.16	Japan	The battery pack caught fire during a Boeing 787 flight from Yamaguchi-Ube to Tokyo
	2014.4	Australia	A Boeing 737 caught fire due to the short-circuit of the battery inside a trunk

These failures could be due to any failure mechanisms outlined in previous sections. For example, the Samsung Note 7 failed and went into runaway due to a fault in the separator. The separator manufactured in the LIB was too thin to increase the energy density but resulted in a greater safety risk of short internal short circuits (50).

Although the failure rate for an electric vehicle (1/10,000 vehicles per year) is lower than a traditional vehicle (7.6/10,000 vehicles per year), the thermal hazards of LIBs continue to hinder the commercial appeal of electric vehicles (50).

The consequence of thermal runaway could vary depending on the cell format and the chemistry. Cylindrical cells and prismatic provide some venting during runaway due to bursting vents allowing the pressure reduction during runaway. However, pouch formats do not have vents and are designed to expand when pressurization occurs during thermal runaway or other phenomena. It
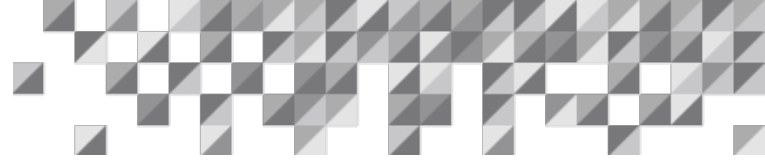
has been recorded that although pouch cells inflate, they can rupture, allowing the vented gases the decomposition, such as the incident documented below.

4.1 BESS Explosion, Arizona

On 19th April 2019, an unexpected explosion of batteries already on fire in a Arizona Public Service's (APS) McMicken BESS site injured eight firefighters. Fluence energy (Fluence) worked with APS to install, configure, and establish operations for APS.

The energy storage system used was LG chem NMC pouch cells stacked together to form each module (51,52). A module contained 28 of these pouch cells packed together. Multiple factors led to the explosion at the site (51,52). The events that led to the incident are outlined below and in Figure 11.

- 16:54:30 the battery voltage dropped off in the 7th battery, module 2 rack 15. (4.06V to 3.82V)
- 16:58:38 the total voltage in rack 15 dropped from 799.9 to 796.1V. BMS loses module level data
- 16:54:40 Temperature readings in the back of rack 15 begin to increase
- 16:55:20 Smoke alarms 1 and 2 in the BESS are detected and the fire protection system is triggered and causes several circuit breakers to open
- 16:55:45 A ground fault was detected
- 16:55:50 The fire suppression system discharges Novec 1230 suppression agent and shuts down the ventilation system
- 16:57 APS contacted Fluence to verify the fire suppression system discharged
- 17:07 Fluence advises APS that its field service engineer in going to provide visual confirmation of the fire
- 17:12 APS dispatches Troubleman to the site to investigate the issue
- 17:40 Fluence field service engineer calls 911
- 17:48 Fire department arrives
- 20:02 Front door opened by emergency responders
- 20:04 Explosion occurs

Sequential factors led to the explosion event outlined in the sequence above. A single cell module initially caught on fire due to an abnormal lithium metal deposition and dendritic growth. This resulted in an internal short circuit leading to a thermal runaway (51). The thermal runaway then propagated
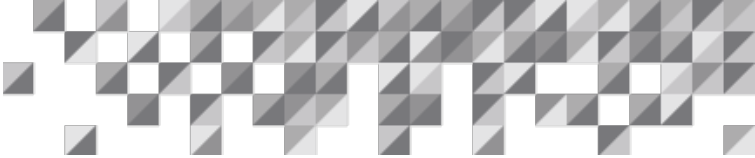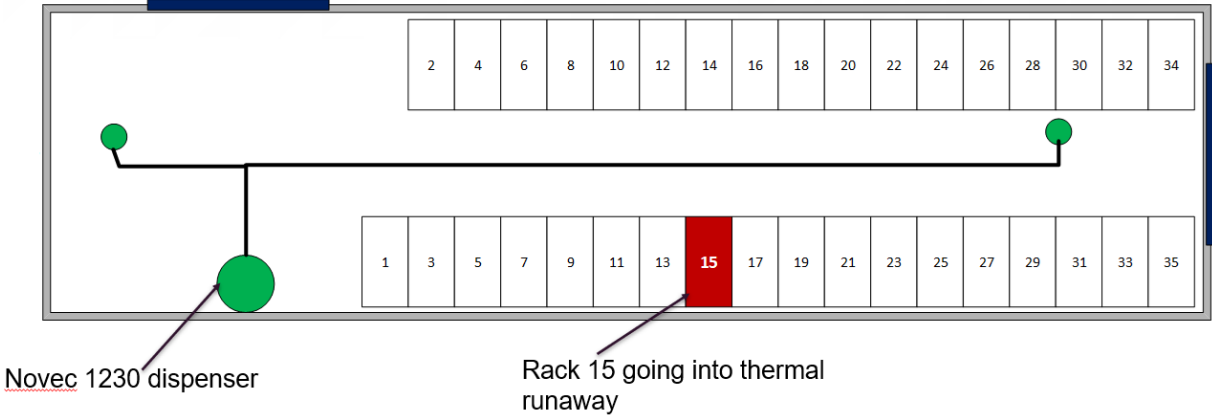
and spread to other modules, as shown in Figure 9. The absence of thermal barriers acted to speed up runaway propagation, and Novec 1230 did not stop the thermal runaway.

Gases accumulated as the thermal runaway progressed between the 911 call and when the responders opened the door. The fire suppression agent played a massive role in the gas accumulation and prevented any ignition of the flammable gases being generated as more and more cells went into a runaway. However, the agent-air mixture dissipated over time, reducing the fire suppression ability.
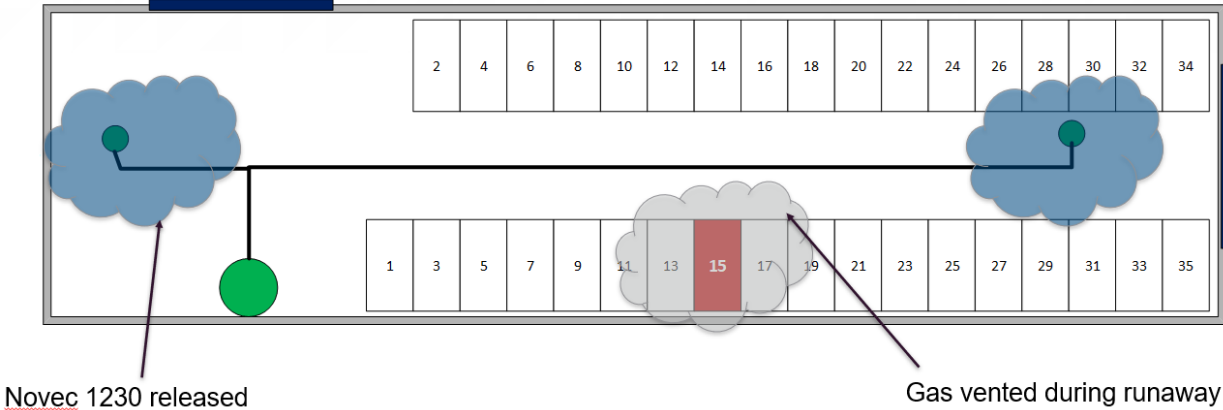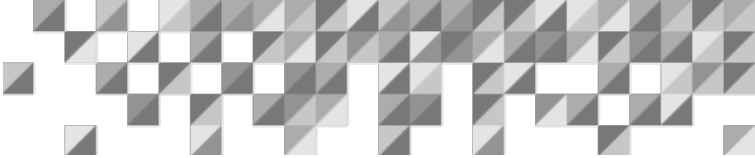
The incident report outlined that the flammable mixture had to have become agitated when the door was opened and encountered an ignition source (53). It is not uncommon for a battery pack to remain hot for several hours after a thermal runaway. Therefore, it could still be possible that the gases could have come into contact with Rack 15 (Ignition source), still hot from thermal runaway as the fuel-rich gas was pushed towards the door resulting in an explosion.

Figure 12 was created assuming that number rack number 15 was approximately in the middle of the LIB distribution, The dimensions of the container were assumed to be like that of a shipping container (51).
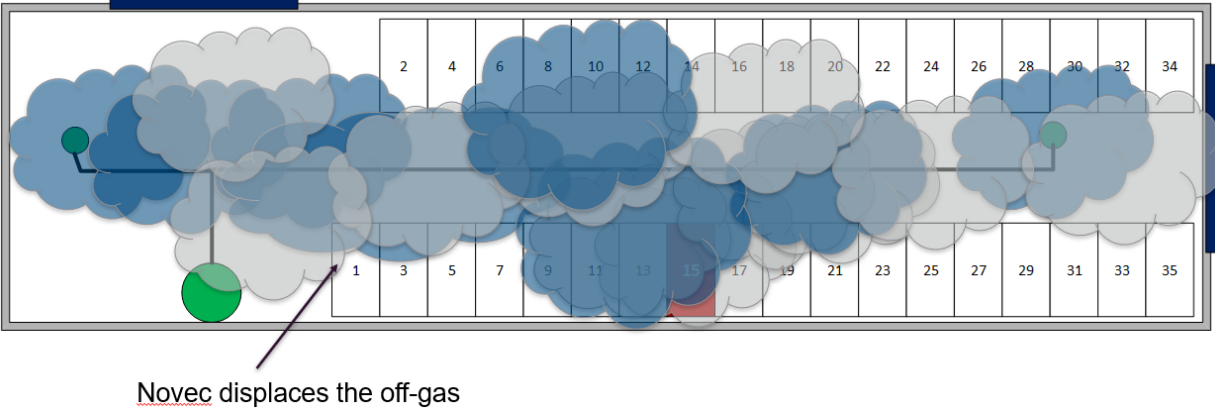
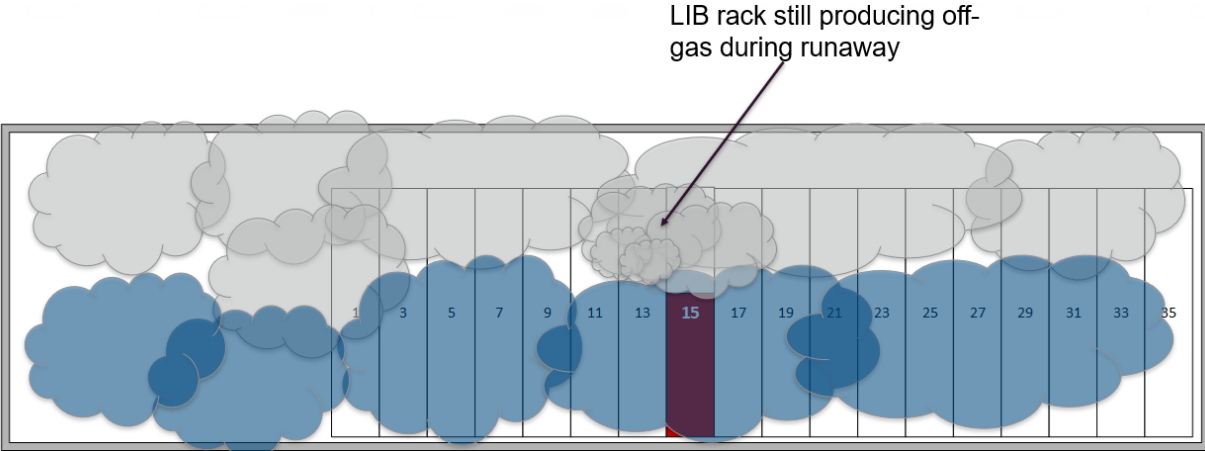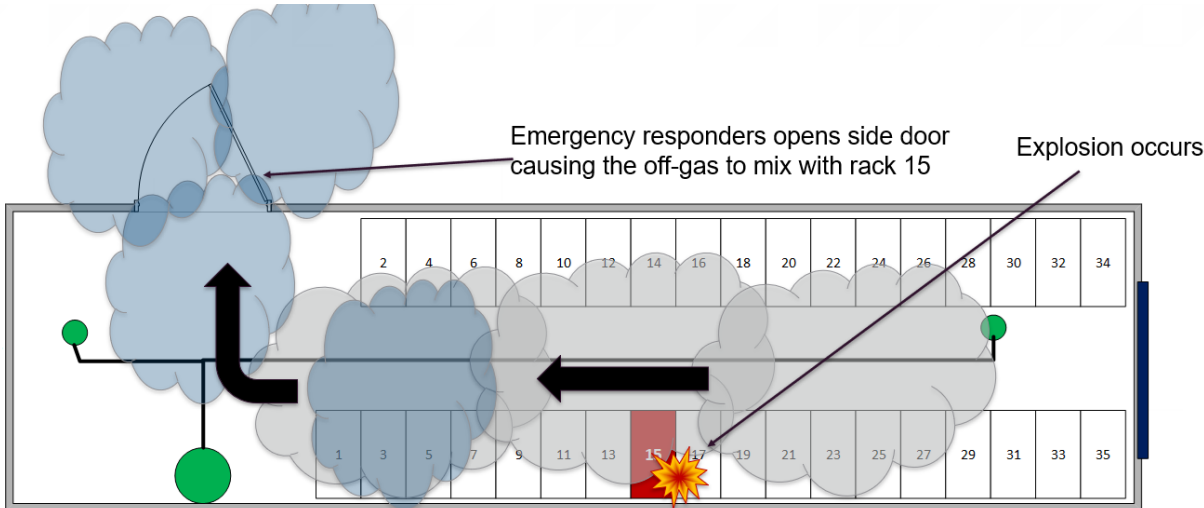## Figure 12: Novec 1230 displacement and cause for explosion

Novec 1230 dispenser

Rack 15 going into thermal runaway

Source: ioMosaic Corporation

Novec 1230 released

Gas vented during runaway

Source: ioMosaic Corporation

Novec displaces the off-gas

Source: ioMosaic Corporation

LIB rack still producing off-gas during runaway
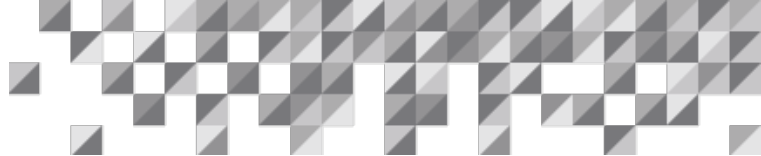
Source: ioMosaic Corporation
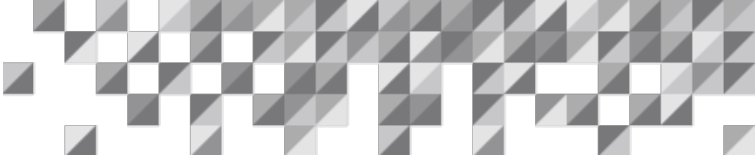
Source: ioMosaic Corporation

5. Modelling 1D Explosion Dynamics in Process Safety Office® SuperChems™

As shown by the explosion of the BESS at the APS site in Arizona, it is essential to adequately size explosion vents of elongated geometries, illustrated in Figure 12. If enough vent gas (off-gas) accumulates, dissipates, and encounters an ignition source, there must be adequate pressure relief to prevent shrapnel from flying from an energy storage container. The confinement caused by the battery racks and other equipment will ultimately result in flame acceleration due to greater surface area being created and compression of the medium, resulting in faster flame speeds.

In the upcoming sections, the BESS case study will be used to explore how Process Safety Office® SuperChems™ can be used to model explosions in elongated geometries. Process Safety Office SuperChems™ can be used to establish flame speed and reduce analytical and acceleration models for the vented gas produced during thermal runaway. We can then define a one-dimensional (1D) geometry like that shown in Figure 12. Using the 1-D explosion dynamics model provides the user with pressure, temperature, and flame speed profiles and the impulse loading on the geometry as shown in Figure 13.

In this model, we can also consider the increase in confinement created by the BESS's racks' blockages. Finally, we can use the 1-D explosion dynamic models to test different vent sizes and locations resulting in optimized sizing. 1-D explosion dynamics is simple and quick in SuperChems™ Expert and provides the same overall answers one might obtain through 2-D modelling but at a far lower financial and computational time cost.

Figure 13: 1-D explosion dynamic model in SuperChems™
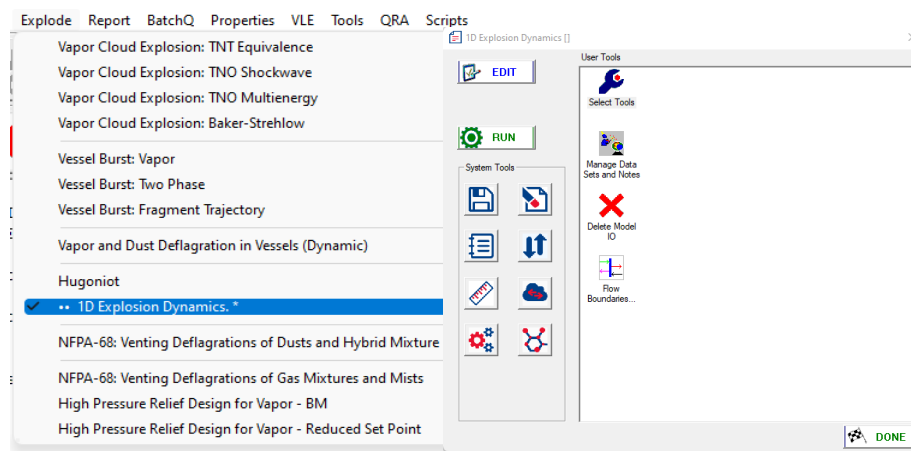
Source: Process Safety Office® SuperChems™ V 11.0
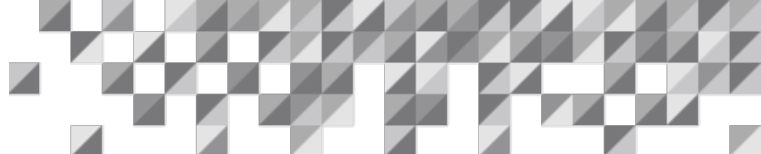
6. Case Study- Example of 1D Explosion Models

6.1 Battery Vent Gas Reduced Analytical model in SuperChems™

The modelling of explosion dynamics for elongated geometries such as energy storage systems requires a detailed calculation for chemical equilibrium to resolve the transient PVT relationship during the explosion. Chemical equilibrium calculations can be time intensive; however, a simplified model can be used with reasonable accuracy.

SuperChems™ can create a reduced analytical model, also known as a constant gamma "γ" model, that can provide an excellent approximation of real fluid results obtained by detailed chemical equilibrium calculations. The reduced analytical model regresses parameters to match the Rankine-Hugoniot solutions produced by more detailed chemical equilibrium calculations (54). Further background and detail on developing reduced analytical models for deflagration can be found in the white paper 'Development of Reduced Analytical Models for Explosion Dynamics'.

For this case study the starting at ambient conditions on the day of the incident in Surprise, Arizona on 19th April, 2019. were approximately 25 ℃ and 1 bar (55).The LIB vent gas is characterized by the contents and chemistry of the cell. To create a reduced analytical model for the vent gas we first need to make approximations to its molar composition. For this case study the gas composition was assumed to be made up primarily of Hydrogen (H_2), Carbon Monoxide (CO), Carbon dioxide (CO_2), Methane (CH_4), and Ethylene (C_2H_4).

Below in Table 3 is the composition used in the incident report (52) and another is from a gas analysis study of a NMC cell of similar chemistry (23) and was used to calculate the volume fractions in the storage system container. Most of the remaining gas was assumed to be Novec1230 and air. Assuming a majority of the Novec1230 was displaced from the room when the door was opened, the model assumes the Novec1230 was in low concentration and the vapor can be adequately modeled with air and the cell off-gas.

The incident report assumed the dimensions of the container to be 50' long, 13' wide and 12' high leading to a total empty volume of 7800 ft^3 (56). Accounting for the equipment inside the room, the interior air volume was determined to be 7062 ft^3 (56). Novec 1230 would occupy 882.9 ft^3 of the available volume. In SuperChems™ we can also determine the LFL of the fuel gas mixture to be 3.605% and UFL is 66.410%.

A constant gamma was regressed and is shown in Figure 14 using the gas in Table 3 with Novec 1230 omitted. Table 4 provides key information from the constant gamma models which are vital to create an explosion model of the incident.
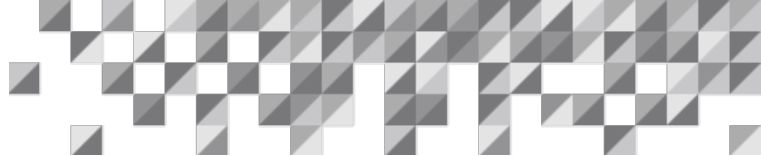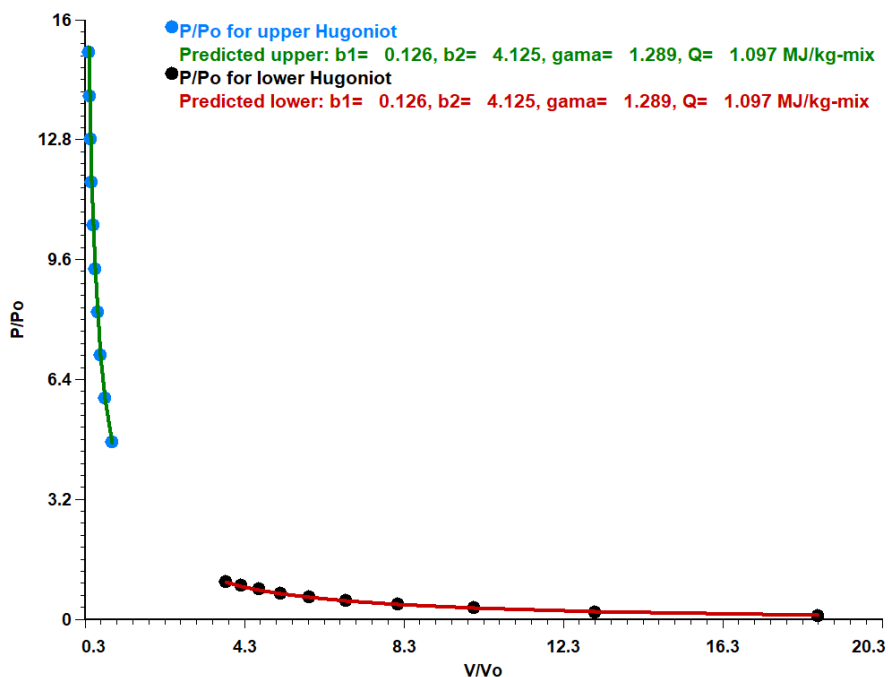
Table 3: Typical Composition from a NMC cell

Component	Golubkov et.al Mol %	Incident report Vol %
Hydrogen (H_2)	30.8	7.4
Carbon Monoxide (CO)	13.0	3.1
Carbon dioxide (CO_2)	41.2	9.9
Methane (CH_4)	6.8	1.6
Ethylene (C_2H_4)	8.2	2.0
Air	N/A	67.5
Novec 1230 ($C_6F_{12}O$)	N/A	8.5

Figure 14: Reduced Analytical models for the cell off gas mixture in air

Source: Process Safety Office® SuperChems™ V 11.0

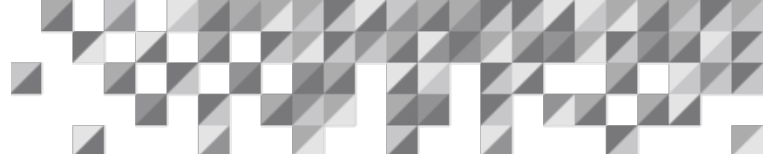Table 4: Key parameters used for the 1D explosion model

Mixture	Heat of Combustion (MJ/kg) Mixture	Constant pressure expansion ratio	γ	Maximum pressure for a constant volume system (psig)
Incident report mixture -no 1230	Novec1.097	3.817	1.289	53.8

6.2 Establishing the 1D Geometry in Process Safety Office® SuperChems™

In SuperChems^{TM} 1D geometries can be created that represent pipelines, vessels and even energy storage system containers such as the one used in the incident in Arizona. The geometry established will be the top-down view of the container and is shown below in Figure 15. The doors were modelled as two boundary conditions, the doors were modelled as ruptured discs relieving when they buckled.

Based on the incident report it was noticed that when the emergency responders opened the front door Novec was displaced. The cell off gas must have been swept over rack 15, for this 1D explosion model and for vent sizing it is assumed that only air and the off gas was in the BESS container.

As described in the incident report both the rear and front doors blew off and based on the geometry and middle position of rack 15 it could be believed that two flame fronts were generated and can be defined as shown in the SuperChems^{TM}.

Rack 15 can be represented as a hot spot within the 1D geometry and is assumed to be at the 25ft mark. The cell chemistry used in the incident report were NMC cells and as shown in Figure 8 single peak temperature can reach up to 600 to 700℃ at which the aluminum casing will begin to yield. Based on tests outlined in the incident report cells which are packed and are allowed to touch can cascade into thermal runaway and trap heat in between cells and range from 300-600 ℃ (56). As shown in Figure 17 when cells cascade and propagate into thermal runaway a high temperature will be maintained between an inside cell. It is assumed that closer to the outer perimeter the temperature is close to atmospheric 25 ℃. For this example, it was assumed that a ramp up in temperature to 600 ℃ at rack 15 occurs. The peak temperature will be changed as part of the sensitivity analysis.
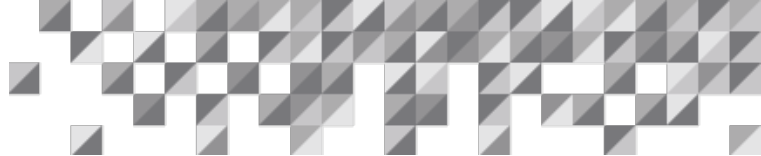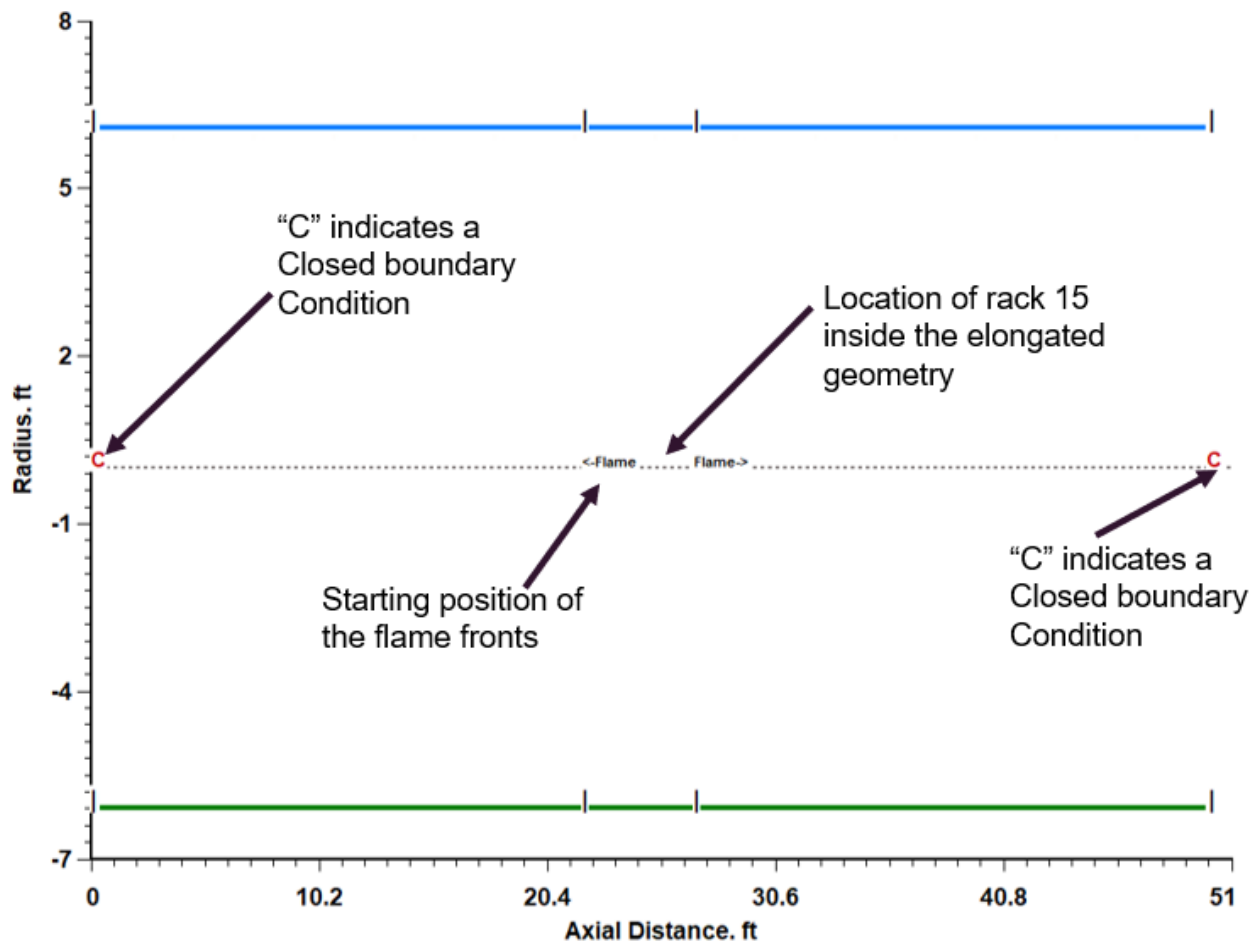
Figure 15: Energy storage system container geometry created in SuperChems™

Source: Process Safety Office® SuperChems™ V 11.0

Boundaries such as closed or open boundaries, rupture discs, blast vents, PRVs mass in and outflow and many more can be defined with specific conditions and allocated anywhere along the 1D geometry in SuperChems™.

For this example, the elongated geometry will have closed boundaries to understand the impulse, reaction force and dynamic temperature, velocity, and pressure rise.

It is assumed no fire suppressant is present in the BESS. The delay of two minutes between the responders entering the BESS chamber and the explosion is most likely when the Novec escaped to the atmosphere therefore, we will be modelling the sudden explosion.
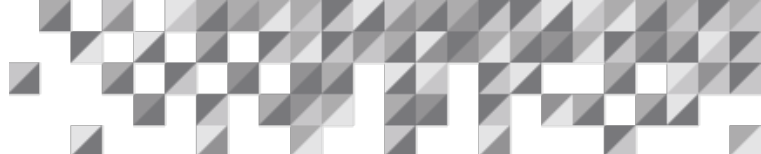
Figure 16: Specifying Initial Conditions Along the 1D Geometry

Source: Process Safety Office® SuperChems™ V 11.0

6.3 Explosion dynamics in Process Safety Office® SuperChems™

The explosion dynamics uses fundamental conservation equations in one dimension over time. The momentum, energy and mass conservation equations are shown by 18-21. The last term allows SuperChems™ to evaluate the partial differential equations with multiple flow boundaries across the elongated geometry making SuperChems™ a useful tool not only for modelling relief load adequacy but position and opening times of blast vents which is equally as important. These boundaries are all scaled requiring less dissipation than previous dynamics models.

We can model the flame front and shock wave throughout the elongated geometry. As the gas gets burnt along the flame front the temperature, pressure, and velocity increases and this will need to
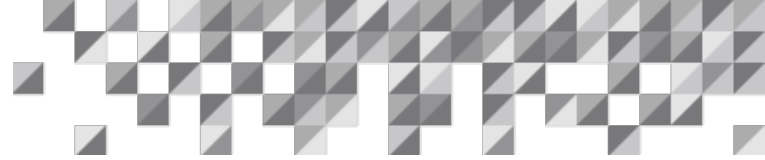
be implemented in the explosion dynamics to accurately represent the impulse loadings and overpressure.

For elongated geometries such as long vessels and energy storage systems (L/D=3.85), flame acceleration can occur due to the presence of obstructions such as cell racks and other equipment (57). Obstructions result in turbulence which accelerates the flame front. In addition to the acceleration effect of a flame front due to turbulence are the acceleration processes of a compressible fluid flowing down a pipe. Generally, compressible fluids will increase their velocity as they move from one end of the pipe to the other. An increase in flame velocity is effectively an increase in reaction rate which impacts the temperature and pressure in the equipment of interest. The Blockage ratio represents how much the flow area is restricted. A maximum blockage ratio of 0.6 is appropriate for the flame acceleration description (57). The white papers 'Quantify Explosion Venting Dynamics in Vessels, Enclosures, and Energy Storage Systems' and 'Laminar Flame Speeds Data Collection. Ensuring reliable data for explosion characterization' provide more detail on how flame speed models are developed and how to define flame acceleration.

It is assumed that the for the following fuel gases the following initial flame speeds can be used. An initial flame speed of 0.35 m/s was used based on the UL laboratories reports (57). Although the case study uses a different composition to the referenced data, this value will be used as a starting point for a sensitivity analysis.

The volume taken up by the equipment was estimated to be 738 ft^3 and can be approximated to a void fraction 0.1 (56). However, what is clear in the photos of the incident, the blockage ratio in terms of the flow area along the BESS is assumed to a be a maximum 0.6. The initial calculations will use a blockage ratio of 0.5.
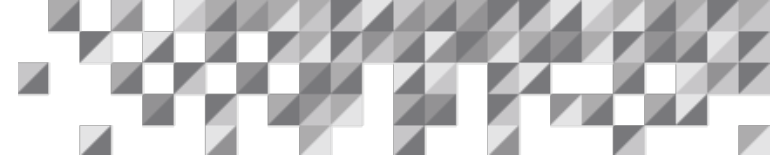
| Description	Mathematical expression	Eq
Continuity equation	$\dfrac{\partial \widetilde{\rho}}{\partial \widetilde{t}} = -\dfrac{1}{\widetilde{A}}\dfrac{\partial}{\partial \widetilde{x}}\left[\widetilde{\rho}\widetilde{A}\,\widetilde{u}\right] + \left[\dfrac{\dot{m}_{in}-\dot{m}_{out}}{A_x \Delta x}\right]\dfrac{t_o}{\rho_o}$	(18)
Energy balance	$\dfrac{\partial \widetilde{T}}{\partial \widetilde{t}} = -\widetilde{u}\dfrac{\partial \widetilde{T}}{\partial \widetilde{x}} + Q\dfrac{S_u}{dx C_v C_o^3} - Q\dfrac{\widetilde{P}}{C_v \widetilde{\rho}\widetilde{A}}\dfrac{\partial}{\partial \widetilde{x}}[Au] + \dfrac{f\widetilde{u}^3}{\sqrt{\frac{\widetilde{A}}{\pi}}C_v} + \dfrac{\widetilde{u}^3}{2C_v}\dfrac{\partial K}{\partial \widetilde{x}} + \nu\dfrac{\partial^2 \widetilde{T}}{\partial \widetilde{x}^2} +$ $\left[\dfrac{\dot{m}_{in}\left(h_{in}+\frac{u_{in}^2}{2}+gz_{in}\right)-\dot{m}_{out}\left(h_{out}+\frac{u_{out}^2}{2}+gz_{out}\right)}{A_x \Delta x \rho_x C_v}\right]\dfrac{t_o}{T_o} - \left[\dfrac{5.67E-08\pi D_x}{A_x \Delta x \rho_x C_v}\left(\dfrac{\epsilon_b \alpha_w}{\alpha_w + \epsilon_b \alpha_w \epsilon_b -}\right)(T^4 - T_s^4)\right]\dfrac{x_o}{c_o T_o} +$ $\left[\dfrac{\pi D_x U(\widetilde{T}_s - \widetilde{T})}{A_x \Delta x \rho_x C_v}\right]\dfrac{x_o^2}{c_o A_o} + \left[\dfrac{k}{\rho_x C_v}\right]\left[\dfrac{\partial^2 \widetilde{T}}{\partial \widetilde{x}^2} + \dfrac{1}{\widetilde{A}}\dfrac{\partial \widetilde{A}_x}{\partial \widetilde{x}}\dfrac{\partial \widetilde{T}}{\partial \widetilde{x}}\right]\dfrac{1}{x_o c_o}$	(19)
Momentum balance	$\dfrac{\partial \widetilde{u}}{\partial \widetilde{t}} = -\dfrac{1}{\widetilde{\rho}}\dfrac{\partial \widetilde{P}}{\partial \widetilde{x}} - \widetilde{u}\dfrac{\partial \widetilde{u}}{\partial \widetilde{x}} - \widetilde{g}\sin\theta - \dfrac{f\widetilde{u}|\widetilde{u}|}{\sqrt{\frac{\widetilde{A}}{\pi}}} + \dfrac{\widetilde{u}|\widetilde{u}|}{2}\dfrac{\partial K}{\partial \widetilde{x}} + \nu\dfrac{\partial^2 \widetilde{u}}{\partial \widetilde{x}^2} + \left[\dfrac{\dot{m}_{in}u_{in}-\dot{m}_{out}u_{out}}{A_x \Delta x \rho_x}\right]\dfrac{t_o}{c_o}$	(20)
Equation of state	$\dfrac{\partial \widetilde{P}}{\partial \widetilde{t}} = -\dfrac{\rho u c^2}{A}\dfrac{\partial A}{\partial x} - uc^2\dfrac{\partial \rho}{\partial x} - \rho c^2 + \left[\dfrac{\dot{m}_{in}-\dot{m}_{out}}{A_x \Delta x}\right]\dfrac{c_o t_o}{\rho_o}$	(21 A)
Ideal gas law	$\widetilde{P} = \dfrac{\widetilde{\rho}\widetilde{R}_g \widetilde{T}}{Mw}$	(21 B)
Nomenclature	A: cross sectional area, c: speed of sound in mixture, Cv: flow coefficient, D: diameter, f: frictional losses, g: gravitational constant, K: pipe losses, Mw: molecular weight, $\dot{m}$: mass flow of fluid, P: fluid pressure, Q: heat input to the system/heat generated in the system, R_g: universal gas constant, S_u: flame speed, T: fluid temperature, Ts: surface temperature for heat transfer, U: universal heat transfer coefficient, u: velocity of the fluid, x: axial position along the geometry, α: heat transfer factor, ϵ: emissivity of a material, θ: angle of geometry relative to the horizontal and ρ: fluid density, ν: thermal diffusivity	
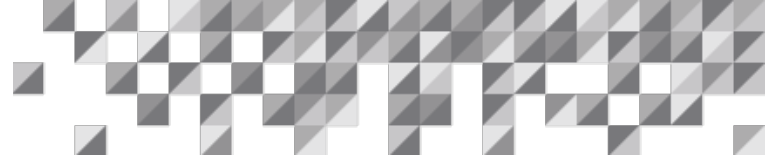
6.4 Explosion Dynamics Results-Closed System

The results show the shock wave propagating along the 1D geometry in both directions; however, the system is assumed to be closed and no mass will enter or leave the system. The pressure waves, temperature and velocity propagate symmetrically due to the initiation of the flame beginning in the middle of the geometry as seen in Figure 17 to Figure 20. The pressure, velocity and impulse can be seen reaching the container wall (closed boundary) within 40ms and reaches a peak overpressure of 1.54 psig and an impulse of 272110 lbf on each side of the front and back walls. At 100ms we reach even higher overpressures at 3.50 psig.

Typically, 1-3 psi in overpressure is enough to result in damage to the container. It was seen from the incident photos the container walls and racks buckled, the rear and side door were forced open, based on photos in the incident report. Although this is a model of a closed system it would stand to believe a quick explosion reaching anywhere from 1-2 psi is appropriate for the scenario due to the extent of the damage. Higher pressures were most likely not reached due to the doors acting as pseudo blast panels providing flow areas for relief.

Figure 17: 1D Pressure Profile
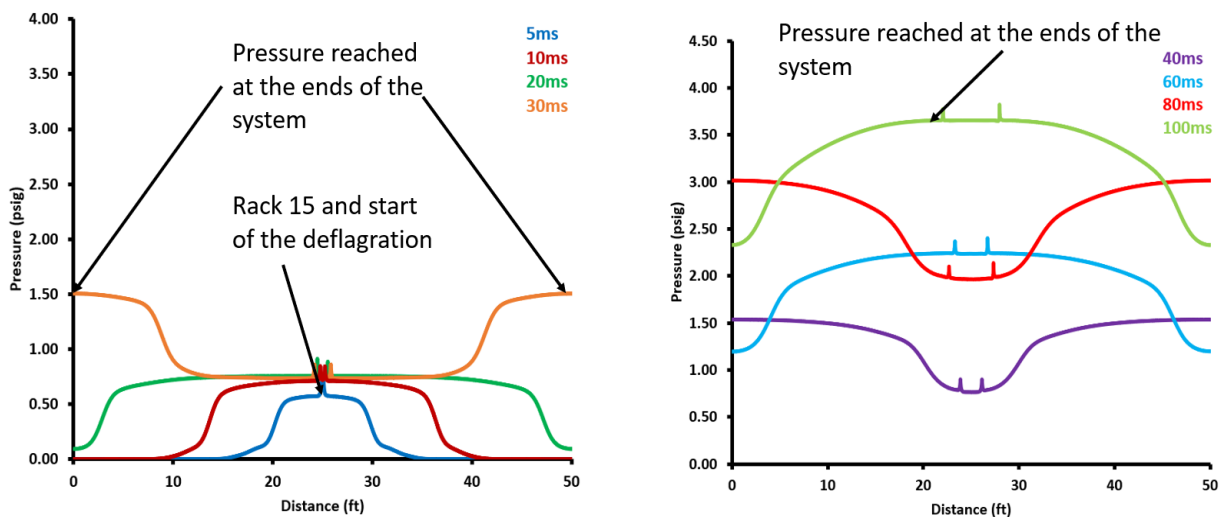
For animated results please click the link: Animation 1: Pressure profile

Source: Process Safety Office® SuperChems™ V 11.0
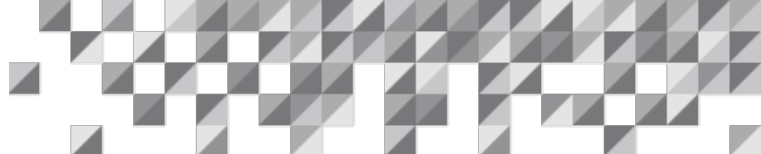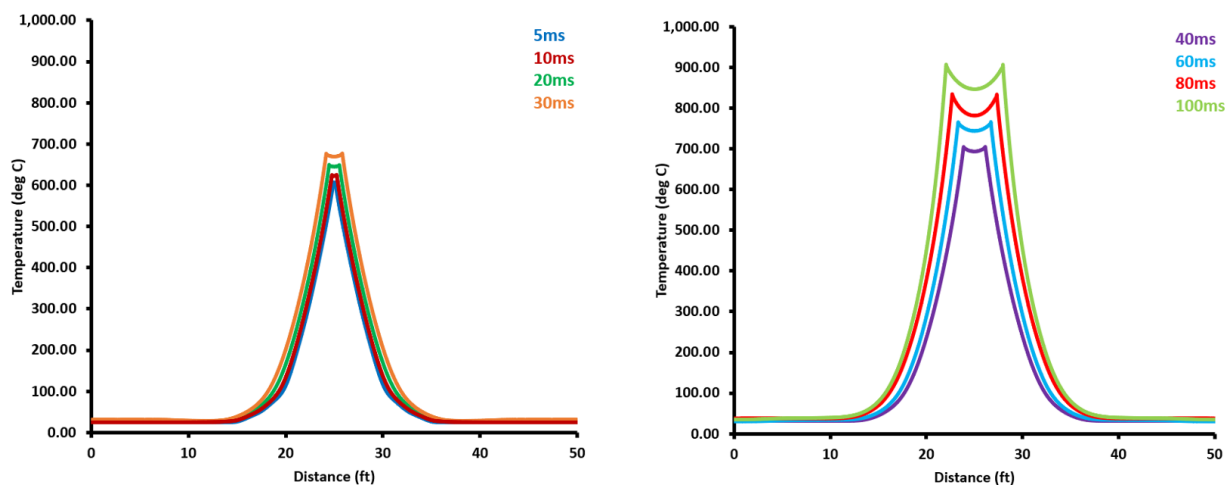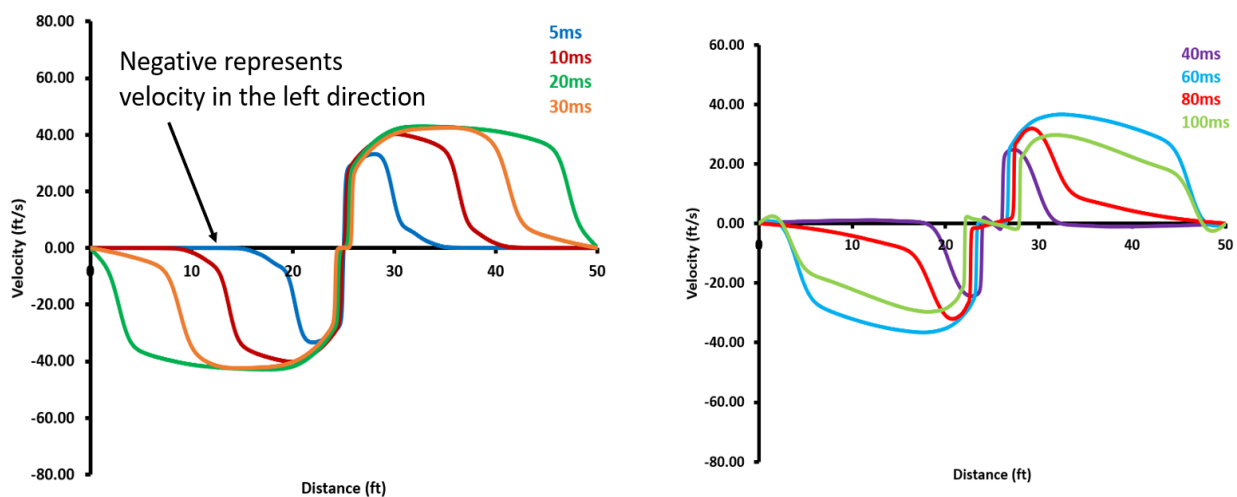
Figure 18: 1D Temperature Profile

Source: Process Safety Office® SuperChems™ V 11.0

Figure 19: 1D Velocity Profile

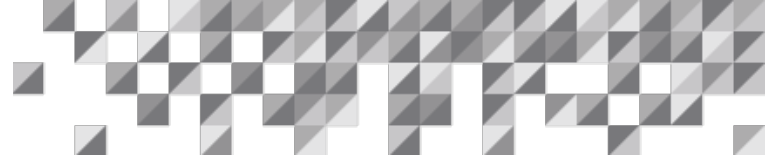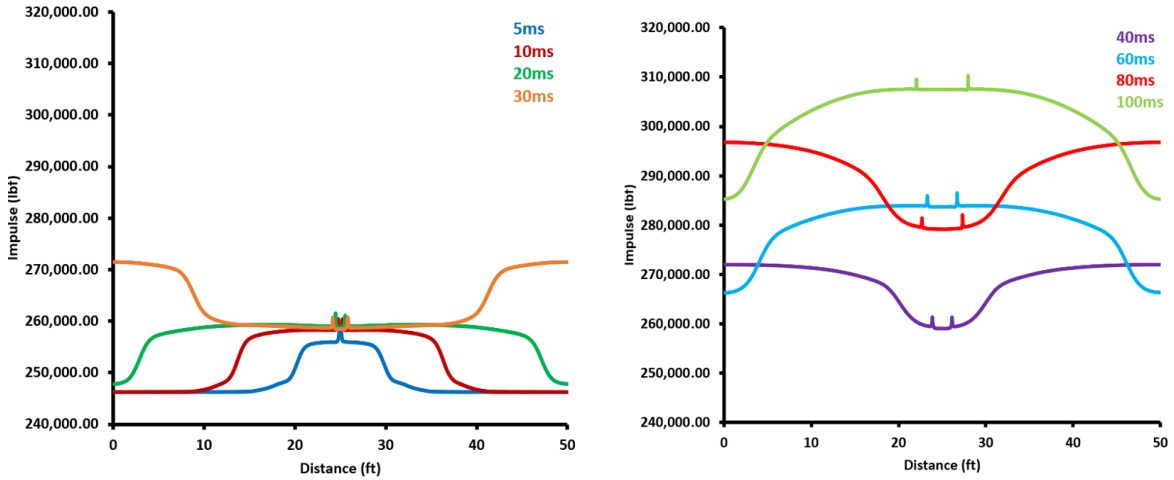Source: Process Safety Office® SuperChems™ V 11.0

Figure 20: 1D Impulse Profile

Source: Process Safety Office® SuperChems™ V 11.0

For a quick analysis the constant gamma model can be used for a prediction of the maximum pressure reached in a closed volume. As shown in Table 4 the maximum pressure reached is 54.5 psig and allowing the 1D dynamics to reaches a maximum pressure in Figure 21 shows good alignment with the maximum pressure predicted by the constant gamma model.

Figure 21: Maximum pressure reached
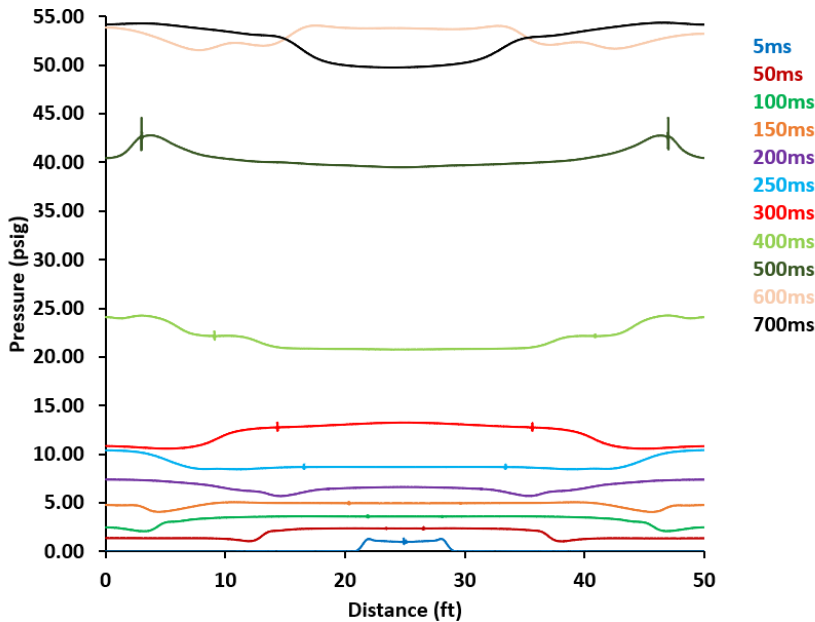
Source: Process Safety Office® SuperChems™ V 11.0
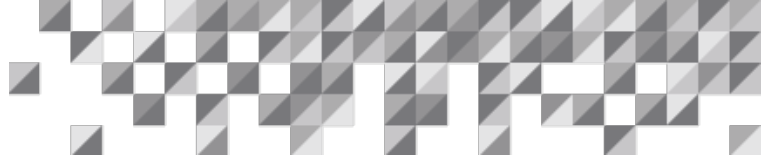
6.5 Explosion Dynamics Sensitivity Analysis

6.5.1 Position

One factor that will impact the impulse load and pressure on the container walls is the position of the deflagration initiation. If we choose rack 25 and 33 as our new positions and focus around 30ms and 60ms we can see the left and right boundary reach peak overpressures at different times as shown in Figure 22.

Figure 22: Pressure Profiles at Different rack Positions at 30ms (Left) and 60ms (Right)
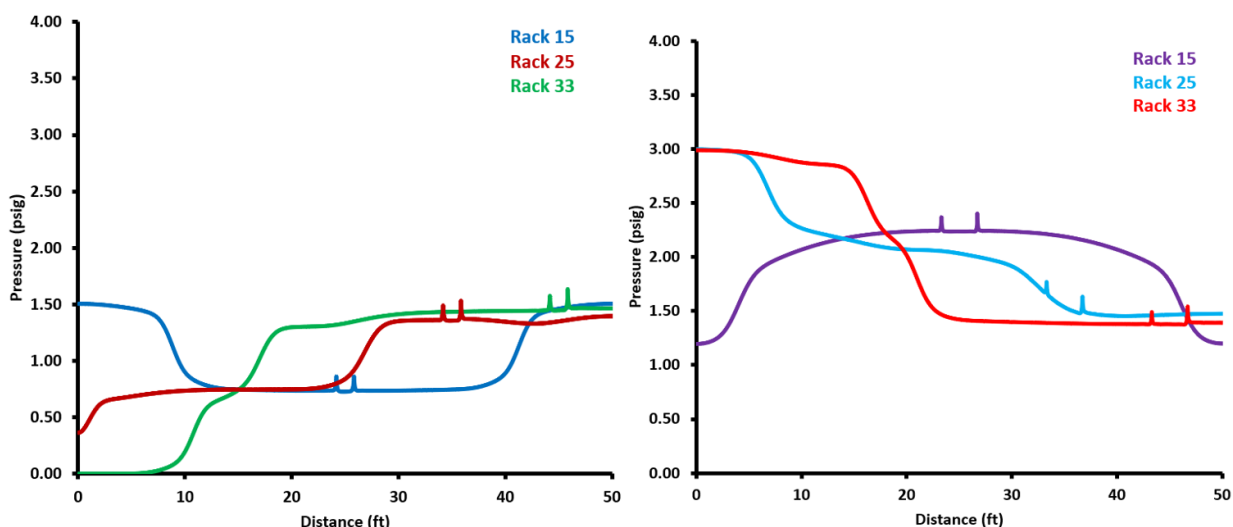
For animated results please click the link: Animation 2: Pressure profile-Rack 25

For animated results please click the link: Animation 3: Pressure profile-Rack 33

Source: Process Safety Office® SuperChems™ V 11.0

6.5.2 Initial Flame Speed

The initial flame speed is a very important parameter and will need to be estimated correctly to provide more accurate values of overpressure and reaction forces on an elongated geometry. The initial flame speed was assumed to be 0.35 m/s based on previous UL laboratory experiments. However, this flame speed was evaluated at a different composition, the UL laboratories off-gas was more equally distributed amongst H_2, CO and CO_2. The higher H_2 concentration could have pushed the flame speed higher, the flame speed provided by UL laboratories was does not appear to be diluted by air which will also have an effect. As shown on Figure 23 the initial flame speed has a large impact.
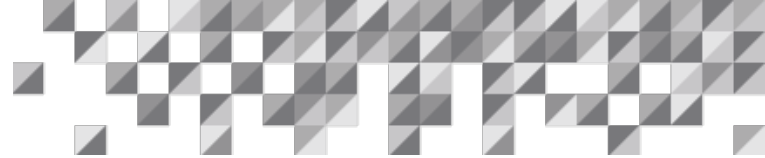
Figure 23: Pressure Profiles at different flame speeds (Left=30ms) and (Right=60ms)
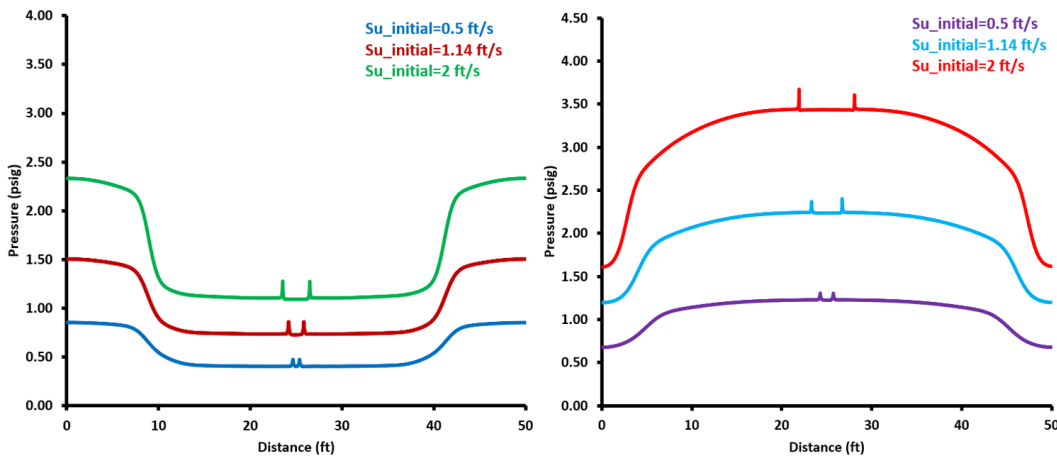
For animated results please click the link: Animation 4: Pressure profile-Uref=0.5m/s

For animated results please click the link: Animation 5: Pressure profile-Uref=2m/s

Source: Process Safety Office® SuperChems™ V 11.0

6.5.3 Rack 15 Temperature

Changing the hot spot temperature results in different peak pressures at the left and right boundary. The lower end of the temperature range of rack 15 outlined in the incident report provided a higher pressure is due to the higher speed of sound calculated in the PDEs 18-21.

Figure 24: Temperature and Pressure Profiles at different Rack temepatures at 30ms (Left=temeprature) and (Right=Pressure)
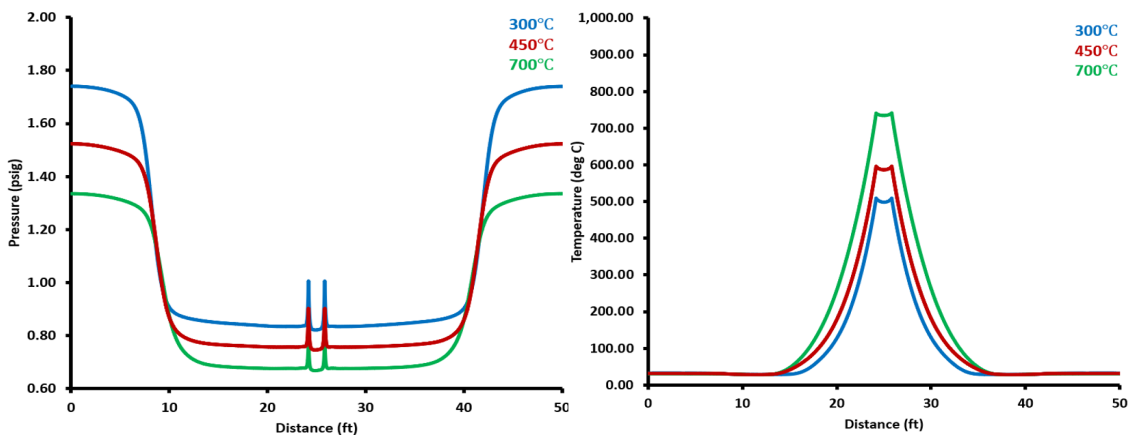
Source: Process Safety Office® SuperChems™ V 11.0

Figure 25: Denisty and Velocity Profiles at different Rack temepatures at 30ms

Source: Process Safety Office® SuperChems™ V 11.0

6.6 Explosion Dynamics with Blast Vents

One method of protecting equipment against deflagration is the use of blast or explosion panels. These panels are designed to burst once a specified pressure has b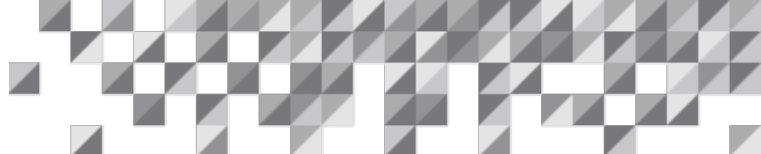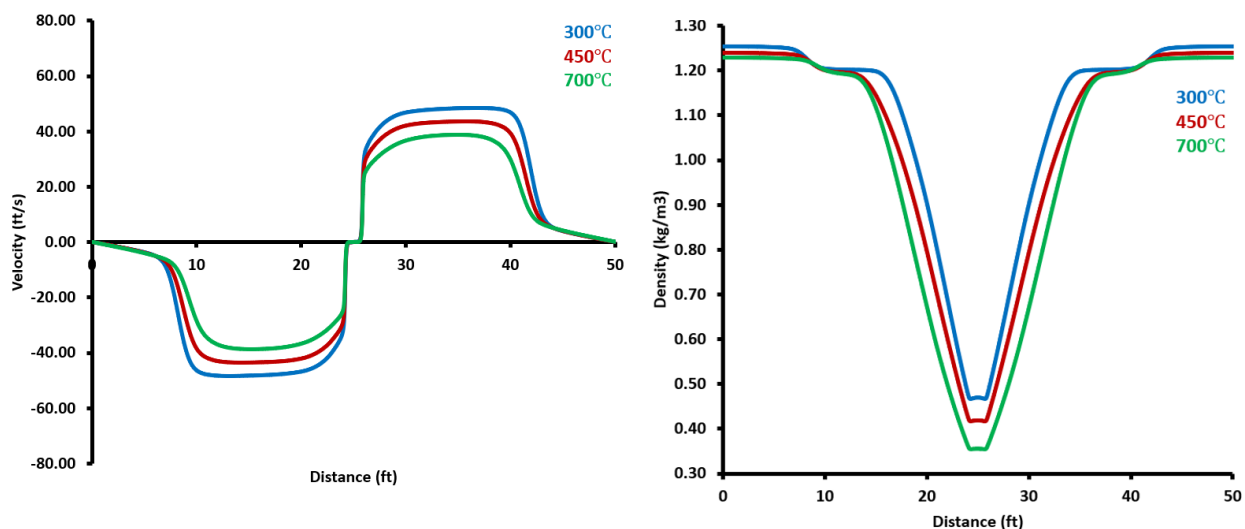een reach and vent the contents of the equipment undergoing the deflagration. Detonations are harder to protect against as the flame speeds move faster than the speed of sound. This has the implication that safety systems that are activated by a pressure value are ineffective when the overpressure event happens at a speed faster than pressure can travel.

It is likely that the doors to the room opened and acted as effective blast panels. Therefore, the pressure computed in the closed system evaluation in Section 6.5. It would be difficult to estimate an exact pressure at which the doors opened however, demonstrating that we can model blast vents it was assumed the doors could be modelled as a blast vent with a set pressure of 1.25 psig which is enough overpressure for the doors to fail. The vent area for one door vent is assumed to be approximately 5000 in^2 which is 25% of the BESS container cross section. In Figure 26 applying blast vents to a 1D geometry is fast and simple.
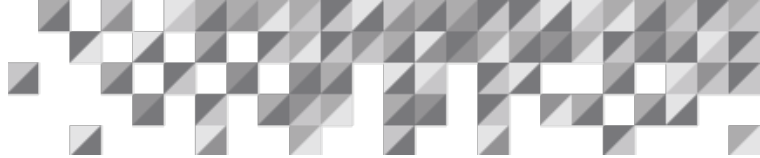
Figure 26: Blast vent (RD) allocation along the 1D geometry a) Blast vents at both ends b) Blast vent at the left boundary and the second closer to the rack.

a)

b)
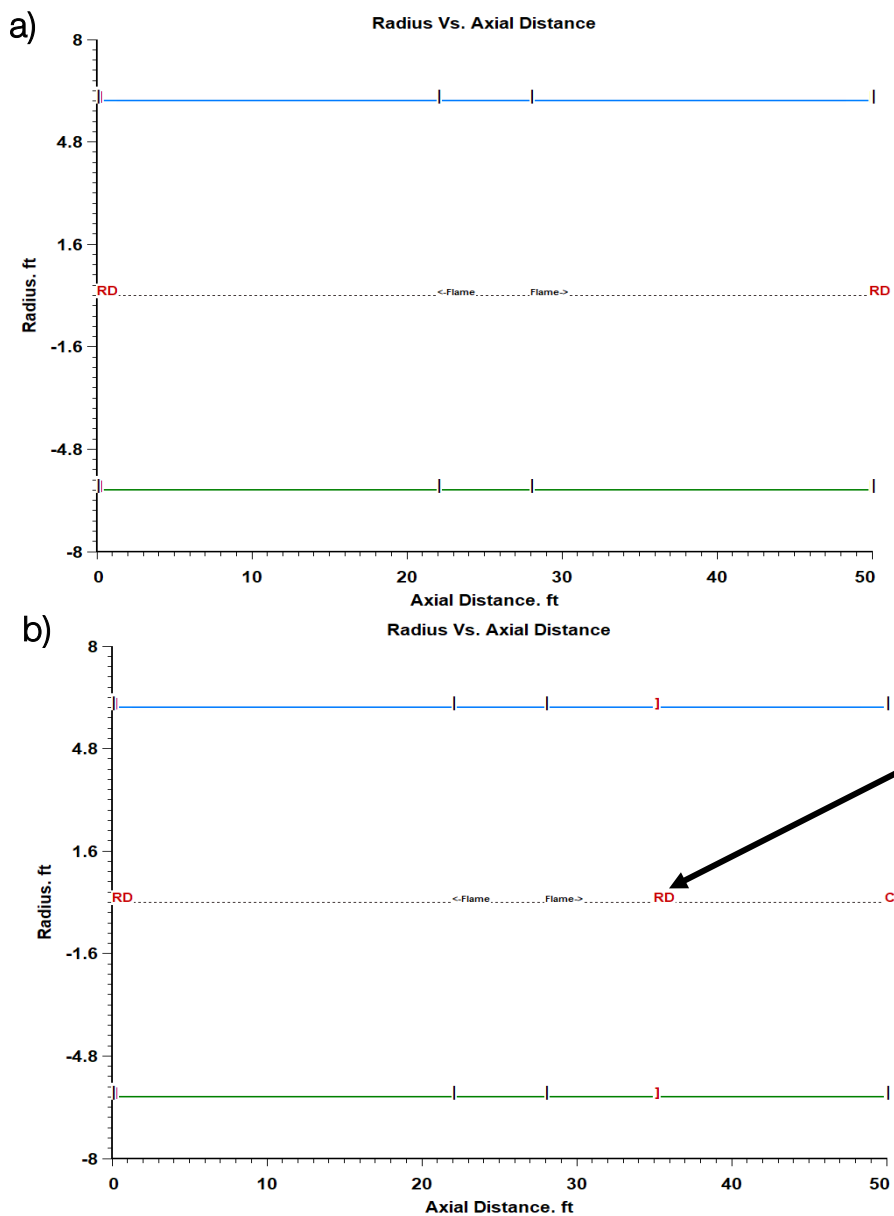
12 boundary conditions can be applied to the geometry and can easily be relocated along the geometry

Source: Process Safety Office® SuperChems™ V 11.0

When the blast vents open on either end the pressure reduces and reaches a steady state. And mass flows out at either side of the geometry. We can also see that changing the blast vent location will change how the pressure waves interact due to the timing of each opening. It can also be seen in Figure 28 that undersized vents results in higher overpressures.
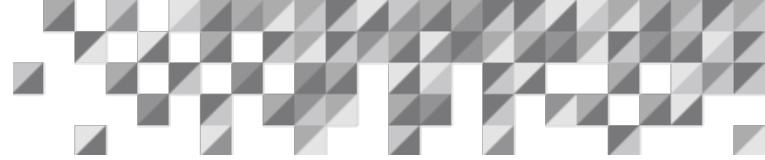
Figure 27: Pressure profiles for configeration (a), when both blast vents (doors) are applied
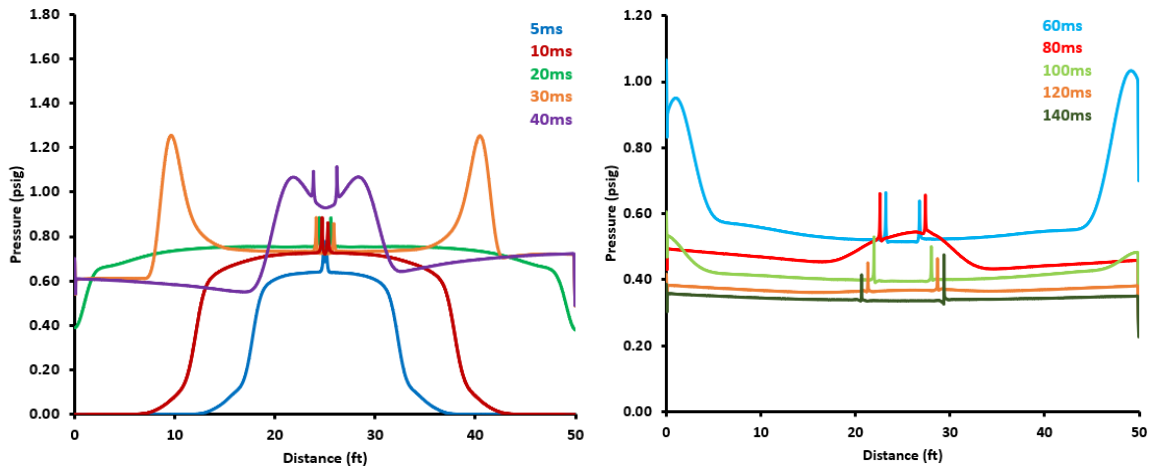
For animated results please click the link: Animation 6: Pressure profile-2 vents

For animated results please click the link: Animation 7: Mass flow profile-2 vents

Source: Process Safety Office® SuperChems™ V 11.0

Figure 28: Pressure profiles for configeration (a), when both blast vents (doors) are applied with lower vent area of 1400 in² per vent
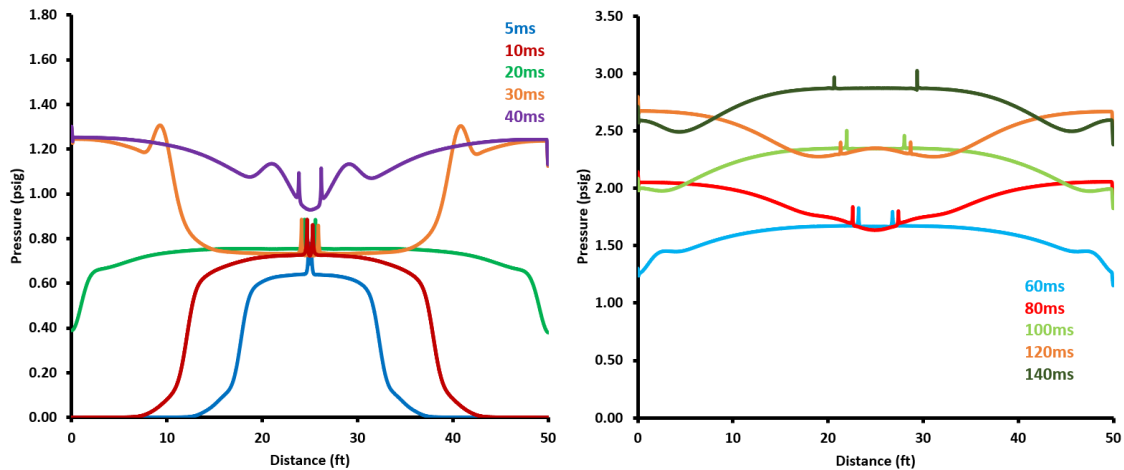
For animated results please click the link: Animation 8: Pressure profile-undersized vents

For animated results please click the link: Animation 9: Mass flow profile-undersized vents

Source: Process Safety Office® SuperChems™ V 11.0
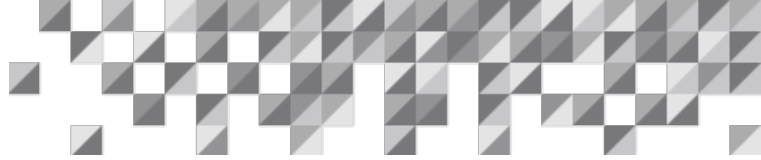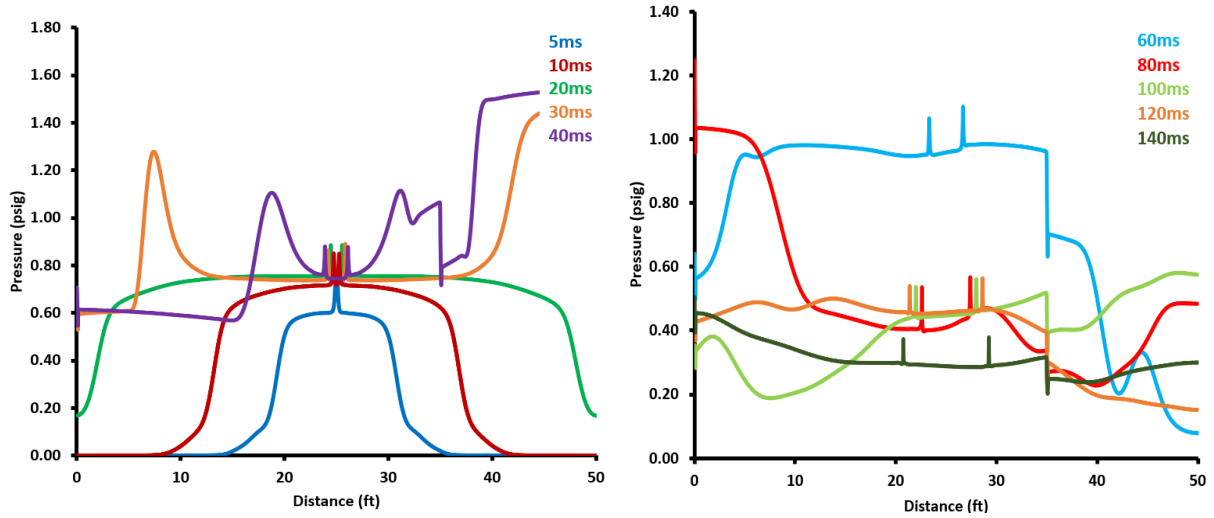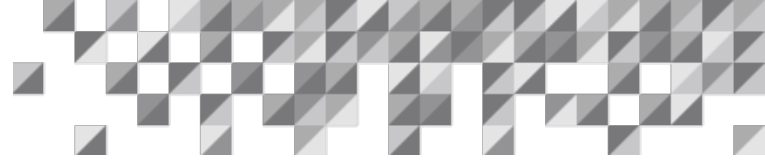
Figure 29: Pressure profiles for configeration (b), when both blast vents (doors) are applied but vent 2 is applied closer to rack 15

Source: Process Safety Office® SuperChems™ V 11.0

7. Conclusions

In this paper it has been shown how 1D dynamics can model deflagration in BESS when a battery thermal runaway occurs. SuperChems^{TM} can adequately size blast panels to reduce the impact of deflagration on the storage system structure by incorporating venting dynamics, burning rate models, defining hot spots, and representing blockages in the geometry. 1D dynamics provides more economically viable and faster computation time than 2D and 3D models for evaluating deflagration, whilst still obtaining the most important, accurate and valuable information when evaluating deflagration scenarios.

SuperChems^{TM} was able to confirm theoretically aspects of the BESS explosion event in Arizona such as Novec 1230 not suppressing the fire in cell rack 15 – possibly due to rapid deflagration meaning that the flammable mixture must have had low concentrations of Novec 1230 inside the container. It can also be concluded from the simulations that doors bucking most likely provided some relief reducing the amount of damage to the container structure.

From this case study a few improvements must be made to reduce the risk of deflagrations and thermal runaways in the future.

1. **Container ventilation and cooling systems**: there must be a means to ventilate the BESS container in a safe manner if release of cell vent gases occurs to maintain the mixture below its lower flammability limits
2. **Incorporate detection systems**: Detection systems that are calibrated to detect specific components can be used to improve response protocols
3. **Research effect cooling between cells and improve battery management systems**: There is current research in module configurations, intercell cooling and heat sink materials which could prevent cell to cell or module to module thermal runaway propagation

ioMosaic and its partner lab has invested in battery testing capabilities such as ARC, abuse testing, DSC and thermal conductivity measurements.1D and higher dimensional thermal explosion models for thermal runaway and propagation characterization are currently being developed. As the world moves towards a sustainable future it is now more important to advance the understanding of battery thermal runaway. ioMosaic's goal is to provide a full scope of modelling and testing capabilities. These models will be an important tool for industrial leaders to use to improve module, pack, and thermal management system designs, the 1D dynamics for deflagration is just one of many yet to come.
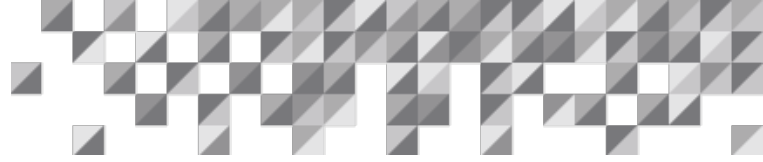
8. Authors

1. James Close; close.j.uk@ioMosaic.com
2. Charles Lea, P.E.; lea.c.mn@ioMosaic.com
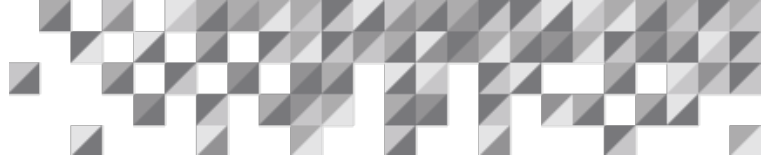
9. References

1. UN D of E and SA. THE 17 GOALS [Internet]. Available from: https://sdgs.un.org/goals

2. Brown Jacob, Oliyide Titi, Petithuguenin Lauren SJ. Maximize value and sustainability in chemicals. The Chemical Engineer. 2021 Oct;(964):18–22.

3. FCAB (Federal Consortium For Advanced Batteries). NATIONAL BLUEPRINT FOR LITHIUM BATTERIES 2021–2030. 2021;(June):1–38. Available from: https://www.google.com/url?sa=t&rct=j&q=&esrc=s&source=web&cd=&cad=rja&uact=8&ved=2ahUKEwiS1LGvssPsAhXZe30KHUvrCUwQFjACegQIARAC&url=https%3A%2F%2Frosap.ntl.bts.gov%2Fview%2Fdot%2F15473%2Fdot_15473_DS1.pdf%3F&usg=AOvVaw31F0kuqTETXYv98O0CuBp_

4. Diouf B, Pode R. Potential of lithium-ion batteries in renewable energy. Renew Energy [Internet]. 2015;76:375–80. Available from: http://dx.doi.org/10.1016/j.renene.2014.11.058

5. AL Shaqsi AZ, Sopian K, Al-Hinai A. Review of energy storage services, applications, limitations, and benefits. Energy Reports [Internet]. 2020;6:288–306. Available from: https://doi.org/10.1016/j.egyr.2020.07.028

6. Stirling T, Stirlin- T. Where you need it, when you need it. Energy Manag.

7. EPA ((Energy Storage Association). Energy and the environment, electricity storage. 2019.

8. U.S. Department of Energy. Battery Storage in the United States: An Update on Market Trends. Batter Storage United States An Updat Mark Trends. 2021;(August):37.

9. A. Otto, S. Rzepka, T. Mager, B. Michel, Fraunhofer, C. Lanciotti, T. Günther OK. Advanced Microsystems for automotive applications 2012. Battery Management Network for Fully Electrical Vehicles Featuring Smart Systems at Cell and Pack Level. 1st ed. G Meyer, editor. Springer; 2012. 18–24 p.

10. Blum AF, Thomas Long Jr R. Fire Hazard Assesment of Lithium Battery Energy Storage Systems [Internet]. 1st ed. Milke JA, editor. New York: Springer; 2016. 21–91 p. Available from: http://www.springer.com/series/10476

11. BEIS. Domestic Battery Energy Storage Systems A review of safety risks. London; 2020.

12. Wang Y-W, Shu C. Hazard Characterizations of Li-Ion Batteries: Thermal Runaway Evaluation by Calorimetry Methodology. In: Zhang Z, Zhang S, editors. Rechargeable Batteries Materials, Technologies and New Trends. 1st ed. New York: Springer; 2015. p. 419–54.

13. Feng X, Ouyang M, Liu X, Lu L, Xia Y, He X. Thermal runaway mechanism of lithium ion
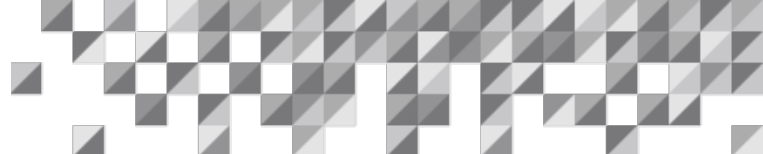
battery for electric vehicles: A review. Energy Storage Mater [Internet]. 2018;10(December 2016):246–67. Available from: https://doi.org/10.1016/j.ensm.2017.05.013

14. Ghiji M, Novozhilov V, Moinuddin K, Joseph P, Burch I, Suendermann B, et al. A review of lithium-ion battery fire suppression. Energies. 2020;13(19):1–30.

15. Feng X, Ren D, He X, Ouyang M. Mitigating Thermal Runaway of Lithium-Ion Batteries. Joule [Internet]. 2020;4(4):743–70. Available from: https://doi.org/10.1016/j.joule.2020.02.010

16. Ostanek JK, Li W, Mukherjee PP, Crompton KR, Hacker C. Simulating onset and evolution of thermal runaway in Li-ion cells using a coupled thermal and venting model. Appl Energy [Internet]. 2020;268(March):114972. Available from: https://doi.org/10.1016/j.apenergy.2020.114972

17. Hatchard TD, MacNeil DD, Basu A, Dahn JR. Thermal Model of Cylindrical and Prismatic Lithium-Ion Cells. J Electrochem Soc. 2001;148(7):A755.

18. Mikolajczak C, White K, Kahn M, Long RT. Lithium-Ion Batteries Hazard and Use Assessment [Internet]. SpringerBriefs in Fire. 2013. 81 p. Available from: http://www.springer.com/series/10476

19. Lisbona D, Snee T. A review of hazards associated with primary lithium and lithium-ion batteries. Process Saf Environ Prot [Internet]. 2011;89(6):434–42. Available from: http://dx.doi.org/10.1016/j.psep.2011.06.022

20. Kong L, Pecht M. A Look Inside Your Battery: Watching the Dendrites Grow [Internet]. Battery Power. 2020 [cited 2022 May 14]. Available from: https://www.batterypoweronline.com/news/a-look-inside-your-battery-watching-the-dendrites-grow/#:~:text=Lithium dendrites are metallic microstructures,into the anode in time.

21. Golubkov AW, Fuchs D, Wagner J, Wiltsche H, Stangl C, Fauler G, et al. Thermal-runaway experiments on consumer Li-ion batteries with metal-oxide and olivin-type cathodes. RSC Adv. 2014;4(7):3633–42.

22. Coman PT, Rayman S, White RE. A lumped model of venting during thermal runaway in a cylindrical Lithium Cobalt Oxide lithium-ion cell. J Power Sources [Internet]. 2016;307:56–62. Available from: http://dx.doi.org/10.1016/j.jpowsour.2015.12.088

23. Austin Mier F, Hargather MJ, Ferreira SR. Experimental Quantification of Vent Mechanism Flow Parameters in 18650 Format Lithium Ion Batteries. J Fluids Eng Trans ASME. 2019;141(6).
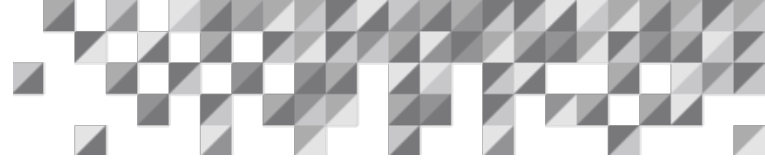
24.   Mier FA. Fluid Dynamics of Lithium Ion Battery Venting. Phd Thesis. 2020;

25.   Kim J, Mallarapu A, Finegan DP, Santhanagopalan S. Modeling cell venting and gas-phase reactions in 18650 lithium ion batteries during thermal runaway. J Power Sources [Internet]. 2021;489(October 2020):229496. Available from: https://doi.org/10.1016/j.jpowsour.2021.229496

26.   Kim JH, Lee KH, Ko DC, Lee SB, Kim BM. Design of integrated safety vent in prismatic lithium-ion battery. J Mech Sci Technol. 2017;31(5):2505–11.

27.   Sheng LH, Zhang S, Zhang Z. Electrolytes for Lithium and Lithium-ion Batteries. In: Zhang Z, Zhang S, editors. Rechargeable Batteries Materials, Technologies and New Trends. 1st ed. New York; 2015. p. 231–61.

28.   Baird AR, Archibald EJ, Marr KC, Ezekoye OA. Explosion hazards from lithium-ion battery vent gas. J Power Sources. 2020;446:1–24.

29.   Li W, Rao S, Xiao Y, Gao Z, Chen Y, Wang H, et al. Fire boundaries of lithium-ion cell eruption gases caused by thermal runaway. iScience [Internet]. 2021;24(5):102401. Available from: https://doi.org/10.1016/j.isci.2021.102401

30.   Zou K, Lu S, Chen X, Gao E, Cao Y, Bi Y. Thermal and gas characteristics of large-format LiNi0.8Co0.1Mn0.1O2 pouch power cell during thermal runaway. J Energy Storage [Internet]. 2021;39(February):102609. Available from: https://doi.org/10.1016/j.est.2021.102609

31.   Zhang Q, Niu J, Zhao Z, Wang Q. Research on the effect of thermal runaway gas components and explosion limits of lithium-ion batteries under different charge states. J Energy Storage [Internet]. 2022;45(July 2021):103759. Available from: https://doi.org/10.1016/j.est.2021.103759

32.   Rickman S, Christie RJ, White RE, Drolen BL, Navarro M, Coman PT. Considerations for the Thermal Modeling of Lithium-Ion Cells for Battery Analysis. 46th Int Conf Environ Syst [Internet]. 2016;(July):1–16. Available from: https://ttu-ir.tdl.org/ttu-ir/bitstream/handle/2346/67474/ICES_2016_9.pdf?sequence=1

33.   Spotnitz R, Franklin J. Abuse behavior of high-power, lithium-ion cells. J Power Sources. 2003;113(1):81–100.

34.   Chen S, Wang Z, Yan W. Identification and characteristic analysis of powder ejected from a lithium ion battery during thermal runaway at elevated temperatures. J Hazard Mater [Internet]. 2020;400(February):123169. Available from: https://doi.org/10.1016/j.jhazmat.2020.123169
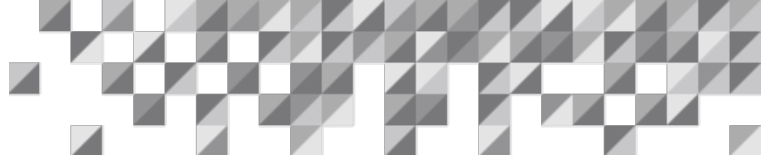
35. Jhu CY, Wang YW, Shu CM, Chang JC, Wu HC. Thermal explosion hazards on 18650 lithium ion batteries with a VSP2 adiabatic calorimeter. J Hazard Mater [Internet]. 2011;192(1):99–107. Available from: http://dx.doi.org/10.1016/j.jhazmat.2011.04.097

36. MacNeil DD, Dann JR. Test of reaction kinetics using both differential scanning and accelerating rate calorimetries as applied to the reaction of LixCoO2 in non-aqueous electrolyte. J Phys Chem A. 2001;105(18):4430–9.

37. Ping P, Kong D, Zhang J, Wen R, Wen J. Characterization of behaviour and hazards of fire and deflagration for high-energy Li-ion cells by over-heating. J Power Sources [Internet]. 2018;398(June):55–66. Available from: https://doi.org/10.1016/j.jpowsour.2018.07.044

38. MacNeil DD, Dahn JR. The Reactions of Li[sub 0.5]CoO with Nonaqueous Solvents at Elevated Temperatures. J Electrochem Soc. 2002;149(7):A912.

39. Chen M, Ouyang D, Weng J, Liu J, Wang J. Environmental pressure effects on thermal runaway and fire behaviors of lithium-ion battery with different cathodes and state of charge. Process Saf Environ Prot [Internet]. 2019;130:250–6. Available from: https://doi.org/10.1016/j.psep.2019.08.023

40. Chen M, Liu J, He Y, Yuen R, Wang J. Study of the fire hazards of lithium-ion batteries at different pressures. Appl Therm Eng [Internet]. 2017;125:1061–74. Available from: http://dx.doi.org/10.1016/j.applthermaleng.2017.06.131

41. Wang Q, Ping P, Zhao X, Chu G, Sun J, Chen C. Thermal runaway caused fire and explosion of lithium ion battery. J Power Sources [Internet]. 2012;208:210–24. Available from: http://dx.doi.org/10.1016/j.jpowsour.2012.02.038

42. Walker WQ, Darst JJ, Finegan DP, Bayles GA, Johnson KL, Darcy EC, et al. Decoupling of heat generated from ejected and non-ejected contents of 18650-format lithium-ion cells using statistical methods. J Power Sources [Internet]. 2019;415(May 2021):207–18. Available from: https://doi.org/10.1016/j.jpowsour.2018.10.099

43. Larsson F, Bertilsson S, Furlani M, Albinsson I, Mellander BE. Gas explosions and thermal runaways during external heating abuse of commercial lithium-ion graphite-LiCoO2 cells at different levels of ageing. J Power Sources [Internet]. 2018;373(July 2017):220–31. Available from: https://doi.org/10.1016/j.jpowsour.2017.10.085

44. Somandepalli V, Marr K, Horn Q. Quantification of combustion hazards of thermal runaway failures in lithium-ion batteries. SAE Int J Altern Powertrains. 2014;3(1):98–104.

45. OutBack Power. UL 1741 SA, Grid Support [Internet]. UL 1741 SA, Grid Support. 2017 [cited 2022 May 14]. Available from: https://www.outbackpower.com/resources-mobile/ul-
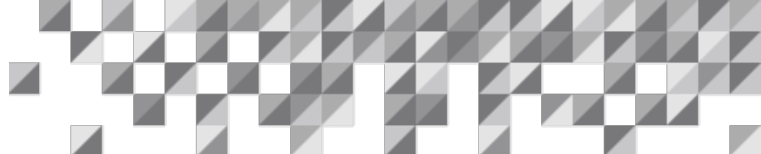
1741-grid-support/ul-1741-sa-gs#:~:text=UL 1741 SA is the,California beginning September 8%2C 2017.

46.	EverExceed Power your applications. Overview of Lithium battery safety testing- UL 1973 [Internet]. web poge. 2021 [cited 2022 May 14]. Available from: https://www.everexceed.com/overview-of-lithium-battery-safety-testing-ul-1973_n433

47.	IEC. IEC 62619:2017 [Internet]. 2017 [cited 2022 May 14]. Available from: https://webstore.iec.ch/publication/28895

48.	Barowy A, Klieger A, Mckinnon M, Regan J, McKnnon M. UL 9540A Installation Level Tests with Outdoor Lithium-ion Energy Storage System Mockups. 2021;1–245.

49.	UL solutions. UL 9540A Test Method [Internet]. 2022 [cited 2022 Aug 24]. Available from: https://www.ul.com/services/ul-9540a-test-method

50.	Ouyang D, Chen M, Huang Q, Weng J, Wang Z, Wang J. A Review on the thermal hazards of the lithium-ion battery and the corresponding countermeasures. Appl Sci. 2019;9(12).

51.	David C. Wagman. Dispute Erupts Over What Sparked an Explosive Li-ion Energy Storage Accident [Internet]. 2020 [cited 2022 Jun 13]. Available from: https://spectrum.ieee.org/dispute-erupts-over-what-sparked-an-explosive-liion-energy-storage-accident

52.	Andy Colthorpe. Arizona battery fire's lessons can be learned by industry to prevent further incidents, DNV GL says [Internet]. Energy Storage News. 2020 [cited 2022 Jun 13]. Available from: https://www.energy-storage.news/arizona-battery-fires-lessons-can-be-learned-by-industry-to-prevent-further-incidents-dnv-gl-says/

53.	SYLVIA T. New reports detail cause of APS battery explosion that left 8 injured [Internet]. PV Magazine. 2020 [cited 2022 Jun 13]. Available from: https://pv-magazine-usa.com/2020/07/30/new-reports-detail-cause-of-aps-battery-explosion-that-left-8-injured/

54.	Melhem GA. Development of Reduced Analytical Models for Explosion Dynamics An ioMosaic Corporation White Paper Development of Reduced Analytical Models for Explosion Dynamics Process Safety and Risk Management Practices. ioMosaic White Pap. 2022;

55.	Weather Spark. April 2019 Weather History in Surprise Arizona, United States [Internet]. 2019 [cited 2022 Jun 14]. Available from: https://weatherspark.com/h/m/2463/2019/4/Historical-Weather-in-April-2019-in-Surprise-Arizona-United-States
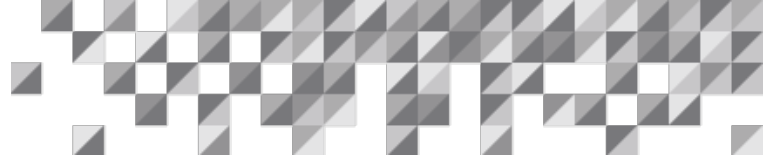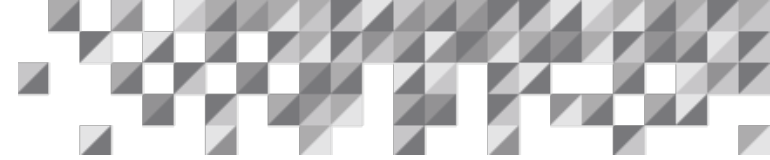
56.   Hill D. Arizona Battery Explosion Exponent DNV-GL FA Report. Rep APS [Internet]. 2020; Available from: https://www.aps.com/en/About/Our-Company/Newsroom/Articles/Equipment-failure-at-McMicken-Battery-Facility

57.   Melhem GA. Quantify Explosion Venting Dynamics in Vessels , Enclosures , and Energy Storage Systems.

58.   Essl C, Golubkov AW, Gasser E, Nachtnebel M, Zankel A, Ewert E, et al. Comprehensive hazard analysis of failing automotive lithium-ion batteries in overtemperature experiments. Batteries. 2020;6(2).

59.   Zhang Y, Wang H, Li W, Li C. Quantitative identification of emissions from abused prismatic Ni-rich lithium-ion batteries. eTransportation [Internet]. 2019;2:100031. Available from: https://doi.org/10.1016/j.etran.2019.100031

60.   Lammer M, Königseder A, Hacker V. Holistic methodology for characterisation of the thermally induced failure of commercially available 18650 lithium ion cells. RSC Adv. 2017;7(39):24425–9.

61.   Golubkov AW, Scheikl S, Planteu R, Voitic G, Wiltsche H, Stangl C, et al. Thermal runaway of commercial 18650 Li-ion batteries with LFP and NCA cathodes - Impact of state of charge and overcharge. RSC Adv. 2015;5(70):57171–86.
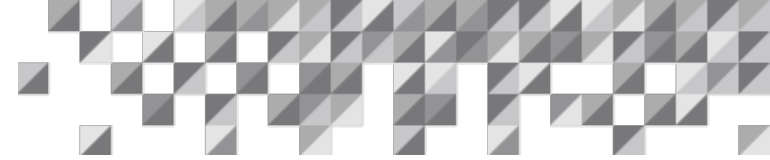
Appendix A: Summary of main components of thermal runaway vent gases from Li W et.al (29)

Table A5: Summary of main components from open literature

Category	#	Name	Formula	Essl et.al (2020) (58)	Zhang et.al (2019) (59)	Lammer et.al (2017) (60)	Golubkov et.al (2015) (61)	Golubkov et.al (2014) (21)	Somandepalli et.al (2014) (44)
Non-HC	1	Carbon dioxide	CO_2	X	X	X	X	X	X
	2	Carbon monoxide	CO	X	X*	X	X	X	X
	3	Hydrogen	H_2	X	X*	X	X	X	X
Alkane	4	Methane	CH_4	X	X*	X	X	X	X
	5	Ethane	C_2H_6	X	X*	X	X	X	X
	6	Propane	C_3H_8	X	X*				X
	7	n-Butane	C_4H_{10}	X	X*				X
	8	Isobutane	C_4H_{10}						**X**
	9	n-Pentane	C_5H_{12}		X*				X
	10	Isopentane	C_5H_{12}						X
Alkene	11	Ethylene	C_2H_4	X	X*	X	X	X	X
	12	Propylene	C_3H_6		X*				
	13	1-Butylene	C_4H_8		X*				X#
	14	2-Methyl propene	C_4H_8		X				X#
	15	trans-2-Butene	C_4H_8		X				X#
	16	cis-2-Butene	C_4H_8		X				X#
	17	1-Pentene	C_5H_{10}		X*				

Category	#	Name	Formula				
	18	cis-2-Pentene	C_5H_{10}		X		
	19	trans-2-Pentene	C_5H_{10}		X		
	20	2-Methyl-1-butene	C_5H_{10}		X		
	21	2-Methyl-2-butene	C_5H_{10}		X		
	22	3-Methyl-1-butene	C_5H_{10}		X		
	23	2-Methyl-1-pentene	C_6H_{12}		X*		
Alkyne	24	Ethyne	C_2H_2	X	X*	X	X
	25	Propyne	C_3H_4		X*		X
	26	1,3-Butadiene	C_4H_6		X*		
Aromatic HC	27	Benzene	C_6H_6		X*		X
	28	Methylbenzene	C_7H_8				X*
	29	Ethylbenzene	C_8H_{10}				X*
	30	m & p-xylene	C_8H_{10}				X
Electrolyte	31	DMC	$C_3H_6O_3$		X*		
	32	EMC	$C_4H_8O_3$		X*		
	33	DEC	$C_5H_{10}O_3$	X	X*		
Others	34	2,4-Dimethyl-1-heptene	C_9H_{18}		X*		
	35	Hydrogen chloride	HCl		X		
	36	Oxygen	O_2	X			

* Substance was used to analyze the temperature boundary and ignition mode.

The type of isomer cannot be determined.